SMTAnews

& Journal of Surface Mount Technology

Volume 33, Issue 1, 2020

Information updated daily... check smta.org for the most current association news.

SMTAnews

Volume 33, Issue 1, 2020

A Message From President, Greg Vance, on COVID-19 Impact

All of us are living through unprecedented times as we manage to deal with the impact of Covid-19. All of us are learning to deal with social distancing, shelter in place orders, non-essential business closures, employee furloughs and the resulting serious impact on our lives and businesses including the SMTA.

Thus far, numerous Expos have been rescheduled and several have been canceled as our chapter leadership and HQ staff deal with the impact of this pandemic. The BoD along with HQ and chapter leadership are continuously reviewing the SMTA calendar and making adjustments as events are cancelled or postponed in order to comply with federal, state, and local group gathering restrictions. Regarding SMTA International, planning continues, and I will keep you posted on any proposed changes. We thank you for taking steps to ensure the safety of our community while trying to preserve the value of the SMTA.

Please know that your BoD and Tanya Martin (Executive Director) are meeting weekly to assess the impact of this pandemic on our organization and reviewing steps to mitigate its effects on the health and financial wellbeing of the SMTA. About event cancellations, we understand that there may be financial obligations that need to be honored. We will work with chapter leadership and the contracted organizations to minimize the financial burden on all.

Please know that what is most important to me, the BoD and HQ staff is the health and wellbeing of our membership and industry partners. We do not know what the coming weeks and months may unfold.

However, we do know that we all should adhere to the federal, state, tribal, and/or territorial guidelines for personal safety while preparing ourselves to react to the dynamic situation as needed in terms of the offerings that we provide through the SMTA.

We recognize there are many unknowns currently, so please share any questions and concerns that you may have with me, your board liaison or SMTA HQ staff. Thank you for all that you do in support of the organization that we all love and care for!

Wishing you peace and health as we work through this challenging time together,
Greg Vance
President, SMTA
Sr. Project Engineer, Rockwell Automation

Listen to Outstanding Speakers Without Leaving Your Desk

SMTA Webinars are a great solution for getting the latest information on electronics assembly and advanced packaging at the best price. View all of our upcoming webinars below and sign up today!

Jul 1, 2020
Dallas Chapter: Modern Conformal Coating – Equipment, Techniques, & Process Issues Webinar

Jul 6, 2020
Solderability Benchmarking, Failures & Production Testing Methods

Jul 8, 2020
Europe Chapter: Systematic Failure Analysis Webinar

Jul 9, 2020
Creating the Best Data Package for PCB Fabrication

Jul 14, 2020
Practical Guidelines in Handling Moisture Sensitive Packages and PWBs

Jul 16, 2020
So You Want to be an Entrepreneur?

Jul 21, 2020
Human Automation: Hands-Free Industry 4.0

Jul 30, 2020
IPC-A-620 "C" to "D" Revision

Aug 10, 2020
Europe Chapter: Monitoring & Benchmarking Your Processes & Assembly Yields Webinar

Aug 18, 2020
How to Minimize Humidity Interaction with PCBAs for Robustness

Aug 20, 2020
Avoiding the Most Common PCB Failure Modes

Aug 26, 2020
Learning to Lead, Leading to Learn

Sep 22, 2020
Europe Chapter: Risk Analysis in Electronic Assemblies Webinar

Members: Vote For Your New Directors
Ballot Closes July 1, 2020

Three positions on the SMTA Board of Directors will be filled for the term 2020-2023. The position of President for a two year term of 2020-2022 will also be filled. This is your opportunity to determine the future direction of your organization. If you are a member, please take advantage of your privilege by voting before July 1, 2020.

All candidates are approved by the Nominating Committee

CANDIDATES FOR PRESIDENT

Martin Anselm, Ph.D.
Rochester Institute of Technology

Tom Forsythe
KYZEN Corporation

CANDIDATES FOR DIRECTOR

MB Allen
KIC

Peter Bigelow
IMI, Inc.

William Capen
Honeywell FM&T

Michael Konrad
Aqueous Technologies

Rajeev Kulkarni
Electronics and Automation

Gregory Vance
Rockwell Automation

SMTA

EDUCATIONAL OPPORTUNITIES

CONFERENCES

One of the ways SMTA enables its members to achieve professional success is by providing unparalleled educational programs and events all around the world. View our website to see the various opportunities available to you.

CERTIFICATION

Gain the most respected sign of approval in the electronics assembly industry! Each SMTA Certification program is a three-day offering consisting of a 1.5-day workshop on topics in SMT Processes followed by open and closed-book exams.

ONLINE TRAINING

Low-cost, self-paced, online training on electronics manufacturing fundamentals. Courses currently available; Stencil Printing, Component Placement, Reflow Soldering, Wave Soldering, Selective Soldering, Rework, and Cleaning.

WEBINARS

Listen to outstanding speakers without leaving your desk! SMTA Webinars are a great solution for getting the latest information on electronics assembly and advanced packaging at the best price. View all upcoming webinars online.

www.smta.org

Expanding Digital Communication

SMTA has been diligently working to increase our online content by working to bring multiple free education tools to our community. This initiative includes a collaborative blog to promote our members' news and research in real-time, as well as the list cultivation of industry related podcasts to promote online-learning.

Additionally, we have updated our YouTube channel to include both full and promo length webinars as a means of encapsulating industry knowledge and in turn, providing education to our members. You can view all of our new uploads on our YouTube channel "Surface Mount Technology Association (SMTA)".

We encourage you to partake in these free tools, and share them with others. If you would like to learn more about this initiative, or wish to contribute your content, please email Tamara Shephard at tamara@smta.org.

New Website Experience Arrives in July

If you haven't heard yet, a new website experience will soon greet you at www.smta.org.

The website launch, scheduled for the evening of July 1st, 2020, will bring a new look as well as a more "social" experience for members.

During the launch, www.smta.org may be unavailable for one to two hours starting at 5:30pm Central Time on Wednesday, July 1st. The new site should be fully accessible and operational by the morning of Thursday, July 2nd.

You will receive an email once the new site is live with instructions for logging in and managing your profile. For security purposes you will need to reset your password the first time you log in to the new site.

If you have any questions about the new website, contact Ryan Flaherty, ryan@smta.org.

SMTA International Conference and Expo Goes Virtual

SMTA International will proceed for 2020 as a completely virtual event starting September 28, 2020.

The decision has been made in light of the COVID-19 pandemic to ensure the health and safety of all those who attend. After reviewing all possible scenarios through weekly meetings with the board, executive director, and venue management, it became clear that an in-person meeting would not be possible given the specific requirements of the state of Illinois, as well as policies restricting travel at many participating companies.

The new virtual format will allow attendees to easily navigate within a simulated conference center environment. Attendees will have access to all keynotes, the exhibit hall, and virtual networking opportunities to interact and collaborate with other participants for a fully immersive experience.

The exhibition is free to all attendees and will take place live September 28 - September 30. During this time, attendees will be able to roam the virtual show floor, view company products and demo videos, and privately chat with exhibitors. Attendees will have continued access to the exhibit hall until October 23, 2020 without the option for live chat.

Attendees who register for the Technical Conference will have exclusive access to over 100 technical presentations on-demand from September 28 - October 23, 2020 as well as the ability to download all papers in the conference proceedings.

The Women's Leadership Program will continue their annual gathering, hosting the Connection Reception on the evening of Wednesday, September 30th.

Further details about SMTA International conference and exhibition are available online at www.smta.org/smtai.

For more information regarding the conference, please contact Karlie Severinson, Events and Administrative Manager, at karlie@smta.org. For inquires about the exhibition, please contact Courtney Kalb and McKenna Hill, Expo Managers, at expos@smta.org.

SMTA International

VISION | INNOVATION | CLARITY

Time to Reconnect

vi·sion

/ˈviZHən/ - noun

1. the ability to think about or plan the future with imagination or wisdom.
   "You will gain clear vison of the future at SMTAI 2020."

2. the ability to interpret the surrounding environment.
   "Accurate vision is needed now more than ever before."

Share Your Vision at SMTA International

smta.org/smtai

Journal of Surface Mount Technology
June 2020 | Volume 33, Issue 1
ISSN: 1093-7358

6600 City W Parkway, Suite 300
Eden Prairie, MN 55344, USA

Phone: +1 952-920-7682
journal@smta.org
www.smta.org

COMMITTEE MISSION STATEMENT

The mission of the SMTA Journal Committee is to select and review papers for publication in the Journal of SMT, ensuring a high standard of quality for each issue and ensuring article content best serves SMTA membership.

Friends, hello from the editorial desk. This is the first issue for the year 2020 even though we have just stepped into summer. In these tough and unusual times where we have expanded our vocabulary with 'social distancing' and are painfully reminded of the presence of racism and 'social injustice,' our reviewers are diligently going about their voluntary service to this Journal. My sincerest kudos and thanks to all of them and to SMTA staff for their exceptional and timely support. I also want to strongly condemn the truly disturbing and ugly prejudice and inequality occurring around us with a gentle reminder that we are all responsible to make this world a better place not only by adding to technical advances but more importantly by eliminating discrimination in any shape or form.

Although we aspire to publish the journal every quarter, we are facing several challenges to do so. First off, we are still climbing the steep learning curve with the new open access system we embraced last year. It has been a tough lesson changing gears from a manual process to cutting our teeth on an automated, on-line system. Secondly, we are still seeking original publications to improve the quality of the journal.

I personally understand how hard it is to work from home, but I also see it as an opportunity to catch up on reviews and technical journals along with a cozy work environment in the confines of your own home office; I gained an hour by not commuting to work. I know many of you are having the same struggles. However, please see the bright side of our circumstances and use your time, wits, and technical wherewithal to pen a paper or two. The Journal needs you.

Finally, in this issue we are presenting three technical topics. Tin whiskers on lead-free solders have always been an issue that worried electronics industry. The first paper studies tin whisker growth on low temperature Bismuth containing lead-free solders under various conditions. Penultimate paper researches defect mitigation through solder joint encapsulation. The last paper explores a novel method to model 'hot tears' that are common in solder joints due to differential cooling during formation.

To submit your original papers to the Journal of SMT, please follow the instructions provided below and send any questions via e-mail to ryan@smta.org.

— *Srini Chada, Ph.D.*
The Journal of SMT Editor/Journal Committee Chair

SUBMIT ORIGINAL PAPERS FOR REVIEW:

1. Go to **https://journal.smta.org** and click "Register"
2. Complete the form to create your profile in the system
3. Once your profile is active, click "Make a Submission"
4. Read all requirements and begin the 5-step process:
    a. Acknowledge and accept the requirements
    b. Upload your paper
    c. Enter metadata
    d. Confirm your submission
    e. Review next steps of the process

Contact Ryan Flaherty with questions: ryan@smta.org

ABOUT THE JOURNAL OF SMT

The Journal of SMT is a quarterly, peer-reviewed, technical publication of articles related to electronic assembly technologies, including microsystems, emerging technologies, and related business operations.

TIN WHISKER FORMATION ON SMALL OUTLINE TRANSISTORS ASSEMBLED USING BISMUTH-CONTAINING LEAD-FREE SOLDER ALLOYS AFTER LONG-TERM AMBIENT TEMPERATURE, HIGH HUMIDITY STORAGE PART 2: STATISTICAL ANALYSIS

André M. Delhaise[1], Stephan Meschter[2], Polina Snugovsky[1], Jeff Kennedy[1*], Zohreh Bagheri[1]
[1]Celestica Inc., Toronto, ON, Canada
[2]BAE Systems, Endicott, NY, USA

ABSTRACT

With the introduction of environmental legislation such as the Restriction of Hazardous Substances (RoHS), lead (Pb)-free materials have made their way into the electronics manufacturing industry. One issue that has emerged is that Pb-free solder alloys can initiate and grow tin whiskers under specific conditions. These whiskers are thin, highly conductive filaments which have the potential to grow and can cause field failures in many applications. Most concerning with respect to tin whiskering are high reliability applications such as aerospace, automotive, and medical.

Bismuth (Bi) is being considered for inclusion in solder alloys to replace the current industry standard (SAC 305) and provide improved thermomechanical and vibration reliability. In this paper, we discuss whisker formation of several Bi-bearing alloys after long-term (12,000 hours), ambient high humidity (25°C/85% RH) storage. Three alloys containing Bi, in addition to SAC 305 (Sn-3.0Ag-0.5Cu), were considered. These alloys were Violet (Sn-2.25Ag-0.5Cu-6.0Bi), Sunflower (Sn-0.7Cu-7.0Bi), and Senju (Sn-2.0Ag-0.7Cu-3.0Bi). The boards were fabricated with electroless nickel immersion gold (ENIG) and immersion tin (ImmSn) finishes and populated with parts having Cu and Fe42Ni alloy leads and chip parts, with half of assemblies cleaned and half cleaned and contaminated with low levels of NaCl.

This paper is the second in a series of three in which we share quantitative statistical analysis from the whisker inspection of the small outline transistor (SOT) components. It was found that on ImmSn surface finishes, the longest whiskers were found on SAC, however the longest whiskers were found on Bi-bearing alloys for ENIG. In addition, whiskers were found to generally grow in regions where the tin coverage is thin, and, on ENIG-finished assemblies, near the PCB, likely due to galvanic corrosion between the solder and the finish chemistry.

Keywords: Tin whisker, nucleation, growth, corrosion, ambient temperature, high humidity, lead-free solder, bismuth, SAC

BACKGROUND

The elimination of lead (Pb) from consumer electronics has resulted in an increased emphasis on tin whisker risk mitigations in aerospace and defense systems using dual-use commercial/aerospace components [1]. Environmental prohibitions of lead in commercial electronics have made these electronic parts and assemblies become more susceptible to tin whiskering. Tin whisker shorting issues were known to be an issue decades ago and at that time whisker issues were solved by the addition of lead into tin. Unlike consumer electronics, aerospace systems can have high consequences of failure and are exposed to many kinds of environmental conditions that promote whisker growth. Some conditions of concern are thermal cycling, vibration, shock, humidity, salt fog, sulfur rich environments, rework, and long term storage. Figure 1 shows several sources of compressive stress in a typical tin plated lead and solder joint.

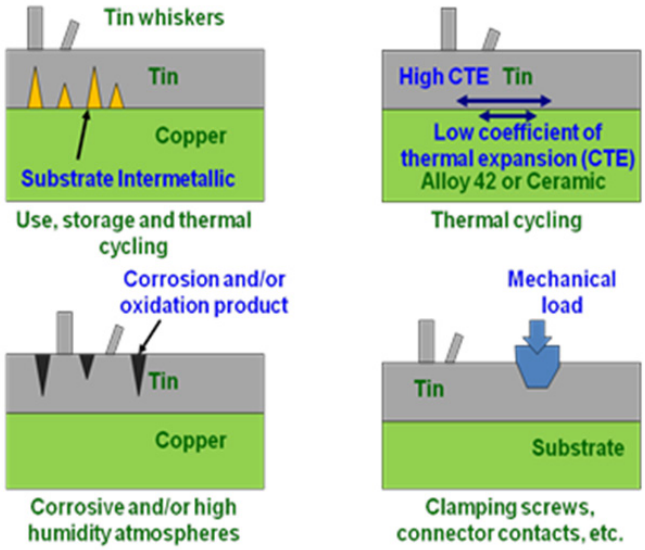

Figure 1: Sources of compressive stress contributing to whisker growth.

The dynamic recrystallization model provides a useful means to describe whisker growth [2]. An interesting aspect of the dynamic recrystallization model is that for a given temperature and grain size if the compressive stress in the tin is either too low or too high, whisker growth does not occur.

Although lead has demonstrated effectiveness at reducing whisker propensity, tin alloying elements can either increase or decrease whisker growth in Sn plating [3][4]. A short duration Sn plating study indicated that Bi addition tended to retard whisker growth

*Currently employed at ZESTRON Americas

considered when evaluating tin whisker growth (e.g. lead material, lead finish, solder alloy, board pad finish, board pad material, and the type/location of intermetallics within the joint) [6]. Solder can have significant whisker growth due to corrosion between different intermetallics in the alloy when contamination is present [7]. The whisker propensity of bismuth containing lead-free alloys in the present evaluation is a lower stress longer term evaluation than the previously completed high temperature high humidity testing [8][9]. Here an 25°C/85 percent relative humidity environment is used, similar to the soldered assembly tin whisker growth test previously performed on SAC305 (Sn-3.0Ag-0.5Cu) [10]. This paper is the second of three parts detailing statistical analysis of whisker growth on the same small outline transistor (SOT) components assembled using bismuth-containing solder alloys shown in the previous paper.

METHODOLOGY

Test Vehicle, Assembly, Cleaning, Contamination, and Exposure

Custom test vehicles were used for whisker growth testing. The individual printed circuit boards (soldered twelve at a time on a panel) are 6 cm x 6 cm x 2.36 mm thick double sided glass epoxy with one ounce copper external base layers and finished with either immersion tin (ImmSn) or immersion gold over electroless nickel (ENIG), both in accordance with IPC-6012.

The types of test vehicles were assembled: SOT (small outline transistor), QFP (quad flat pack) and BGA/CAP (ball grid array/capacitor). Only the SOT boards (Figure 2) are considered in this paper; part types on this test vehicle are given in Table 1. The boards on the panels were soldered using solder pastes composed of the alloys and flux shown in Table 2. The SAC305 assemblies were soldered with a peak reflow temperature of 240 °C, while the bismuth containing alloys had a peak reflow temperature of 226 to 228 °C (as measured at the board surface).

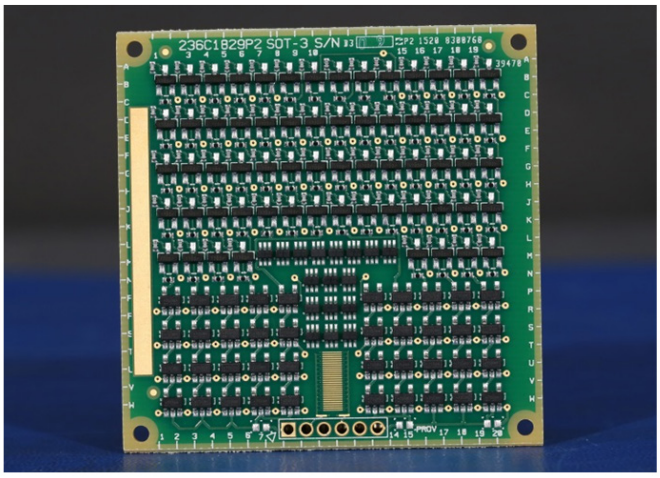

Figure 2: SOT test vehicle.

After soldering, the boards were cleaned with a conventional in-line cleaner. Next, selected boards were re-contaminated by immersion in pans with solution of 160 ppm NaCl in deionized water. Based on prior work, the resulting assembly contamination level of the purposely contaminated assemblies is expected to be near 5 ppm Cl- by ion chromatography with a total concentration of approximately 12 µg/in^2 equivalent Cl- as measured by resistivity of solvent extraction [10]. Assemblies were exposed to low temperature high humidity (ATHH) 25°C/85% relative humidity (RH) simulated long term storage.

Table 1: SOT board parts.

Designation Part No. Package	Lead Frame (4)	Lead finish	No. of leads per part / No. of parts
SOT3 2N7002 (1) SOT23-3	Alloy 42	Matte Sn	3/64
SOT5 NC7S08M5X (2) SOT23-5	Cu194	Matte Sn	5/40
SOT6 2N7002DW-7-F (1) SOT363	Alloy 42	Matte Sn	6/17
R0402 0402- Pb-free Chip resistor	Alumina	Matte Sn	2/128
Notes: (1) Fairchild; (2) Diodes Inc.; (3) Practical Components (Amkor); (4) From the manufacturer's data sheet Alloy 42 is Fe39-41Ni-0.6Mn-0.05Cr-0.02Si-0.05C and Cu194 alloy is Cu 2.1-2.6Fe 0.015-0.15P 0.05-0.2Zn			

Table 2: Solder assembly alloys and fluxes.

Solder	Composition (weight percent)	Flux
SAC305	96.5-Sn, 3-Ag, 0.5-Cu	INDIUM8.9HF
Senju M42	94.25-Sn, 2-Ag, 0.75-Cu, 3-Bi	INDIUM8.9HF
Sunflower	92.3-Sn, 0.7-Cu, 7-Bi	INDIUM8.9HF
Violet	91.25-Sn, 2.25-Ag, 0.5-Cu, 6-Bi	INDIUM8.9HF

For further details concerning these processes, please refer to the corresponding section(s) in Part 1 of this paper series.

Whisker Inspection

A Hitachi S-3000 scanning electron microscope (SEM) was used for the inspection and an electron dispersive X-Ray (EDX) was used for elemental analysis. The first inspection was performed after 1,000 hours. Following the inspection, the samples returned into the chamber and re-inspected after an additional 3,000 hours for a total of 4,000 hours (1,000h + 3,000h). Then the samples were returned to the chamber again and re-inspected after an additional 8,000 hours for a total of 12,000 hours (1,000h + 3,000h, + 8,000h).

This series of papers describes the inspection on selected parts from the SOT assemblies. The boards were inspected to obtain whisker nucleation and length statistics. An inspection was done for each combination of alloy (SAC, Senju, Sunflower, Violet),

surface finish (ENIG, ImmSn) and level of cleanliness (clean and contaminated). All or portions of the following short hand may be used to reference the configuration: (Finish-Solder-Board-Part-Reference Designator-Lead).

At the 4,000 inspection interval, the following quantities of randomly selected parts were inspected at 4,000h for each combination:

- SOT3 – 6 components, 18 leads
- SOT5 – 2 components, 10 leads
- SOT6 – 2 components, 12 leads

At the 12,000 inspection interval, the same part locations for each combination were examined. The following quantities were inspected:

- SOT3 – 8 components, 24 leads
- SOT5 – 5 components, 25 leads
- SOT6 – 4 components, 24 leads

SEM photographs of all regions on the leads were taken at 100x magnification and all visible whiskers were counted to obtain whisker density. The whisker length criterion in JESD22A121A was used to perform the whisker length measurements [13] in the SEM, except whisker nucleation sites having an aspect ratio of approximately one were included in the whisker count. Whiskers longer than 10 microns were measured.

A unique aspect of measuring whiskers on part solder joints is that nothing is planar and the sample must be continually rotated and tilted during the inspection. As the stage is tilted, the whisker length appears to increase until the SEM inspection azimuth angle is perpendicular to the whisker. Further tilting results in the whisker beginning to appear shorter. In the present work, the reported whisker length measurements are conservative. During the length measurement procedure, the SEM inspection azimuth axis was adjusted to be aligned to within ~30 degrees from perpendicular to the whisker. The SEM axis misalignment from the whisker normal results in a potential whisker length under-reporting of up to 15 percent as shown in Figure 3. All whisker dimensions are reported in microns.

The whisker location was documented in an effort to understand patterns related to the underlying metallurgy. The locations are defined in Figure 4; the surface areas of each joint (lead, pad, and solder joint fillet) with respect to locations obtained via the image post processing are provided in Table 3. These surface areas were used in density calculations and were previously determined in earlier SERDP work [9]. In the present experiments, all whisker growth in region 2 occurred where the solder was thin, unless otherwise noted. Whisker diameter was also measured in the SEM. In addition, the whisker growth angle was approximately measured as shown in Figure 5.

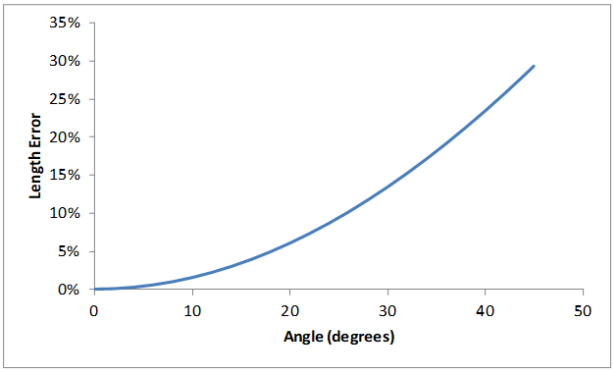

Figure 3: Whisker length measurement error estimate.

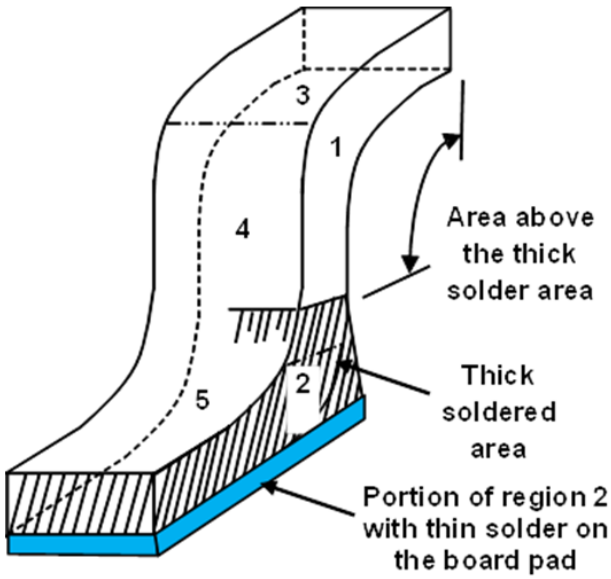

Figure 4: Whisker location definition. The hatched region 2 indicates the thick solder region on the lead and includes the thinner solder that wet onto the board pad. Areas 1, 3, 4 and 5 represent the thin solder or tin region above the thick solder area.

Table 3: Computed areas for SOT whisker growth locations (mm²).

Location	SOT-3	SOT-5	SOT-6
1	0.086	0.187	0.116
2	0.572	0.573	0.358
3	0.066	0.054	0.036
4	0.066	0.212	0.117
5	0.314	0.241	0.133
Total	1.104	1.267	0.760

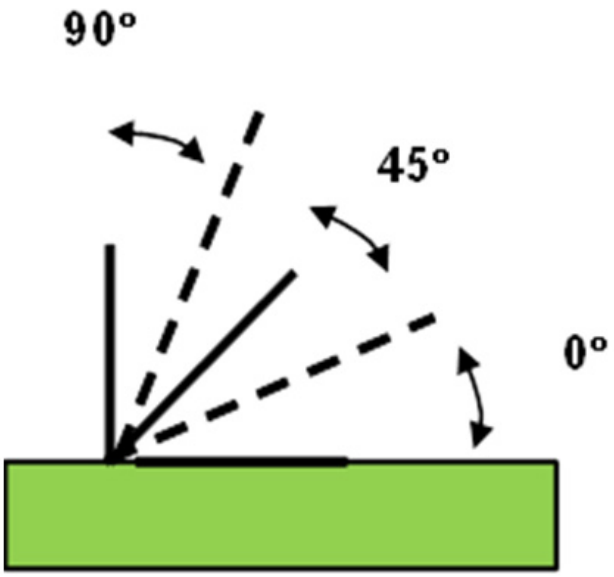

Figure 5: Whisker angle measurement definition.

INSPECTION RESULTS

1000 and 4000 hour inspections

At the 1000 hour inspection, the cleaned boards had no whisker growth. The contaminated assemblies demonstrated growth of several small whiskers; the longest observed was 12 microns in length and was found on a SOT-5 component assembled using Sunflower paste on immersion tin finish.

After 4000h, only a few whiskers were observed on contaminated assemblies. Cleaned assemblies did not grow any whiskers. No whiskers failed JESD Class 2. The longest whisker was on ImmSn-SAC 305-SOT3, and was 29.5 microns in length and was hollow. Only four whiskers greater than 10 microns were measured; the only one that was not hollow was 11.9 microns in length, on ImmSn-Senju-SOT3. The longest whisker from the 1000 hour screening inspection was not observed in the 4000 hour screening inspection because a different set of parts were inspected.

12,000h inspection

General Observations

More whiskers were observed on contaminated assemblies than cleaned assemblies, and a larger proportion of parts/leads on ImmSn assemblies had whiskers compared with ENIG (Figure 6). For both cleaned and contaminated assemblies, a larger fraction of the inspected parts and leads assembled with Bi-bearing alloys (particularly Violet and Sunflower) demonstrated whisker growth than those assembled with SAC 305. Notably, for cleaned ENIG assemblies, whiskers were only observed on Sunflower, and on cleaned ImmSn assemblies, the proportion of parts/leads with whiskers increased with Bi content. A similar trend was observed on contaminated assemblies.

Whisker Length

The vast majority of whiskers greater than 10 microns in length were on contaminated parts – only one such whisker (14.3 microns) was observed on a cleaned assembly (ImmSn, Violet, SOT5, at L3 (Location 3, ref. Figure 19 in Part 1).

On contaminated ImmSn, two whiskers were measured which failed JESD201 for temperature/humidity storage. These measured 98.4µm and 79.3µm respectively and were found on SAC and Senju SOT-3 parts, respectively. Long whiskers on SOT-3 also occurred on the high temperature/humidity samples from our earlier work [9]. All alloys and parts showed comparable ranges in measured whisker length other than a few outliers such as those mentioned above – this indicates that whisker length is much more consistent on Bi-bearing alloys and the risk of developing a long whisker is reduced (Figure 7).

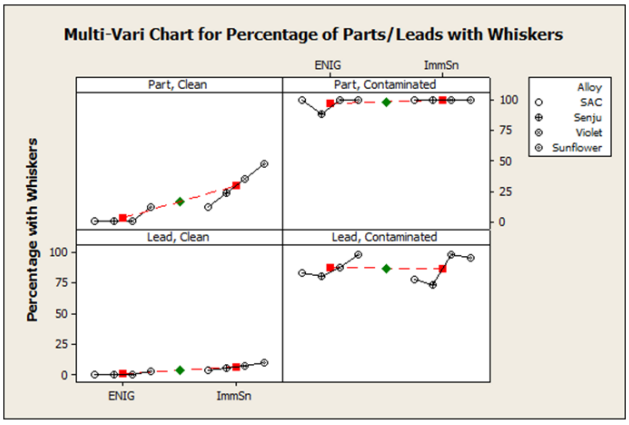

Figure 6: Percentages of inspected parts and leads with whiskers, by assembly cleanliness, surface finish, and alloy.

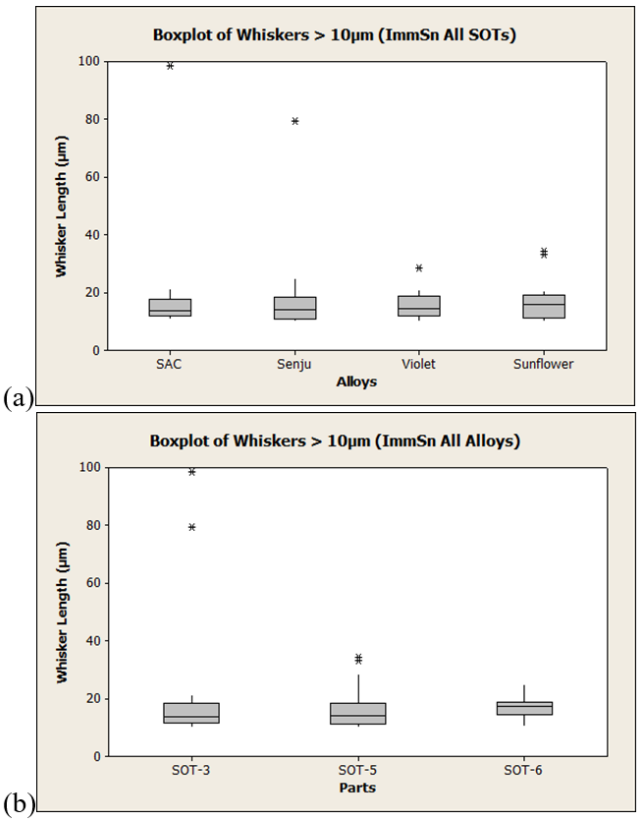

Figure 7: Statistical distribution of measured whiskers on the ImmSn finished boards; (a) alloys and (b) part types.

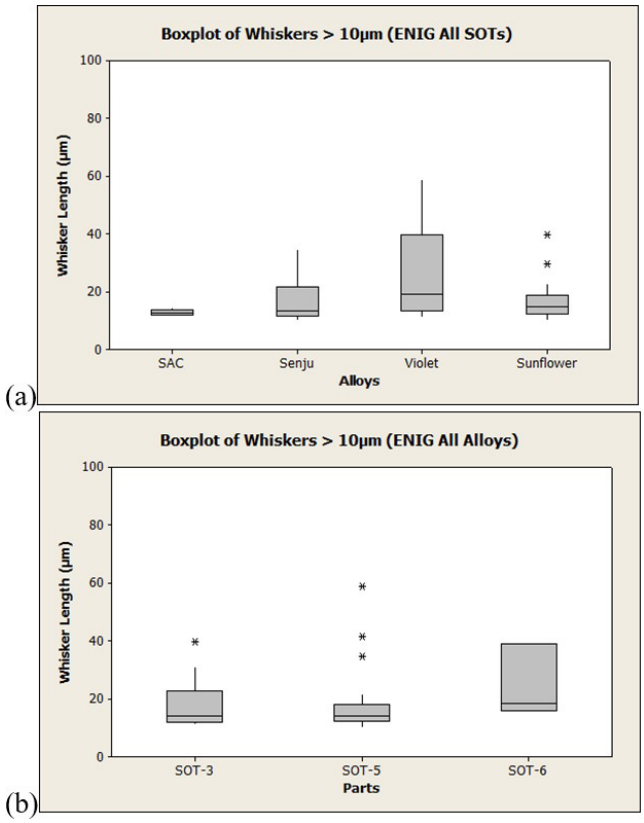

Figure 8: Statistical distribution of measured whiskers on ENIG finished boards; (a) alloys and (b) part types.

A very different trend was observed on ENIG (Figure 8). SAC showed very few whiskers longer than 10µm in length, and two whiskers on Violet SOT-5 parts failed the JESD standard (58.7 and 41.4µm). Two additional whiskers on Sunflower SOT-3 (39.7µm) and Violet SOT-6 (39.1µm) nearly failed. Overall, fewer whiskers greater than 10µm in length were measured on ENIG than on ImmSn, however Sunflower had the most of the four alloys.

Whisker Density

Whisker density data is presented in a multiple-variable chart in Figure 9, with each panel consisting of combinations of surface finish and assembly cleanliness, with data points grouped by alloy with respect to location. Almost all whiskers on cleaned assemblies were present at L1, L3, and L4 and on SOT-5 and 6 parts; these leads are taller than SOT-3 leads and locations are near the top of the lead, where the solder is thinner, which are ideal conditions for whiskering. With respect to location and part type, all four alloys showed varying distributions of whisker density, most notably Violet and Sunflower for ImmSn. These 'spikes' in density can be explained by the localized concentration of whiskers on a small number of the total cohort of inspected leads. For example, the high density seen on Sunflower L1 is the result of 29 whiskers observed on one SOT-5 lead, 2 whiskers on another SOT-5 lead, and zero whiskers on the remaining 23 leads. Similar trends occurred for Violet; in both cases the leads with high whisker count were heavily corroded (Figure 10, also seen in Part 1). It is suspected that the contamination/corrosion may be the result of handling between chamber exposures. However, there are times when high whisker density occurred on the clean assembly with little or no incidental contamination (Figure 20 in Part 1 showing Imm Sn-Sunflower-SOT5-U18 lead 4).

It is recommended that either the exposure time be increased to grow more whiskers, or a larger number of parts/leads be inspected for more meaningful data analysis of the cleaned assemblies.

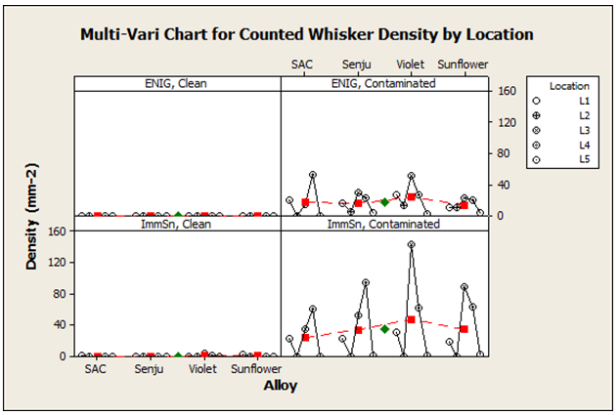

Figure 9: Whisker density by location, organized by assembly cleanliness, surface finish, and alloy.

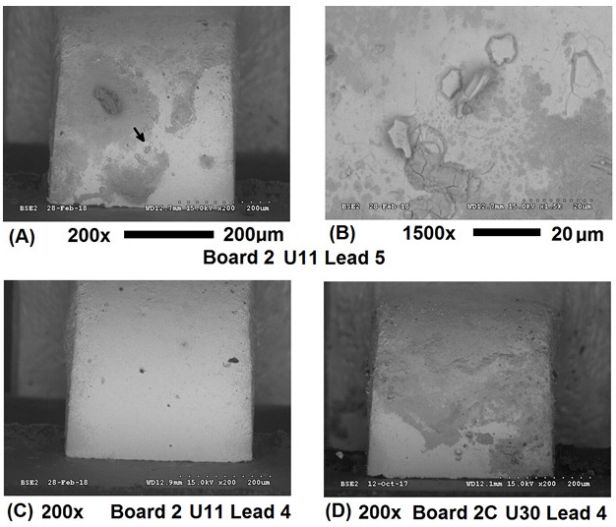

Figure 10: High whisker growth and corrosion on a cleaned assembly on a Violet soldered SOT5 lead on an ImmSn board, corresponding to the large spike in Figure 10. (A) Overview of lead, (B) whisker growth near the arrow in A, (C) adjacent lead with no corrosion or contamination, and (D) typical lead corrosion and whisker growth on a purposely contaminated assembly.

Similarly to the cleaned assemblies, whiskers were found almost exclusively on L1, L3 and L4 on contaminated ImmSn assemblies. The trend in density with respect to location varied between alloys. For SAC and Senju, the higher whisker density was on L4, and for Violet and Sunflower, the highest whisker density was on L3. Minor differences in density between the alloys are observed for L1 and L4 (other than Senju L4). Examination of Alloy-Part-Location plots with respect to whisker density did not explain these differences – for each alloy, different part types were more favorable to whisker. It can be said that there are many competing processes taking part in these samples which make interpretation of the results difficult.

Two significant observations can be made comparing the ENIG result to the ImmSn result – fewer whiskers overall were seen on ENIG, and on the Bi-bearing alloys, appreciable whiskering was observed on L2 and L5, which did not show any whiskers on ImmSn. This may be a corrosion effect exclusive to the ENIG finish and is discussed below. In addition, a greater ratio in density between L3 and L4 was observed for the Bi-bearing alloys.

There appears to be a shift in the density difference between lead frame materials (Alloy 42 and Cu194) as the Bi content in the alloy increases (Figure 11). On both ImmSn and ENIG assemblies, higher densities are observed on Cu194 for SAC 305. Generally, Bi-bearing alloys demonstrate slightly higher density on Alloy 42 compared to SAC, and the whisker density on Cu194 is lower. ImmSn Senju is one interesting exception – density is higher than on any other combination of alloy and lead frame for ImmSn. For Violet and Sunflower, Alloy 42 demonstrated higher whisker density than Cu194, the opposite to what was seen for SAC.

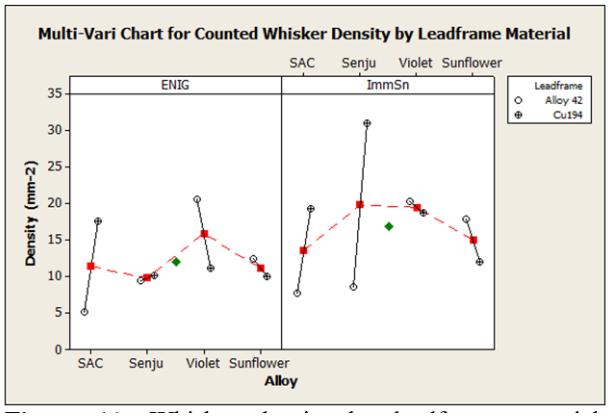

Figure 11: Whisker density by leadframe material, organized by surface finish and alloy.

Whisker density was calculated for each lead and these values (except densities of zero) are plotted in Figure 12 (ENIG) and Figure 13 (ImmSn), for each alloy and plot type, and fitted to a lognormal distribution. Statistical results from these distributions are given in Table 4 (ENIG) and Table 5 (ImmSn).

Definitions of the parameters are as follows:

- N: Number of leads with a whisker density.
- Location: Indicative of the median (log scale) whisker density.
- Scale: Indicative of the distribution of data (log scale). A larger value indicates a wider spread in whisker density across the sampled leads.
- AD (Anderson-Darling statistic): Indicative of how well the data fits the lognormal distribution. A larger value indicates a poorer fit.

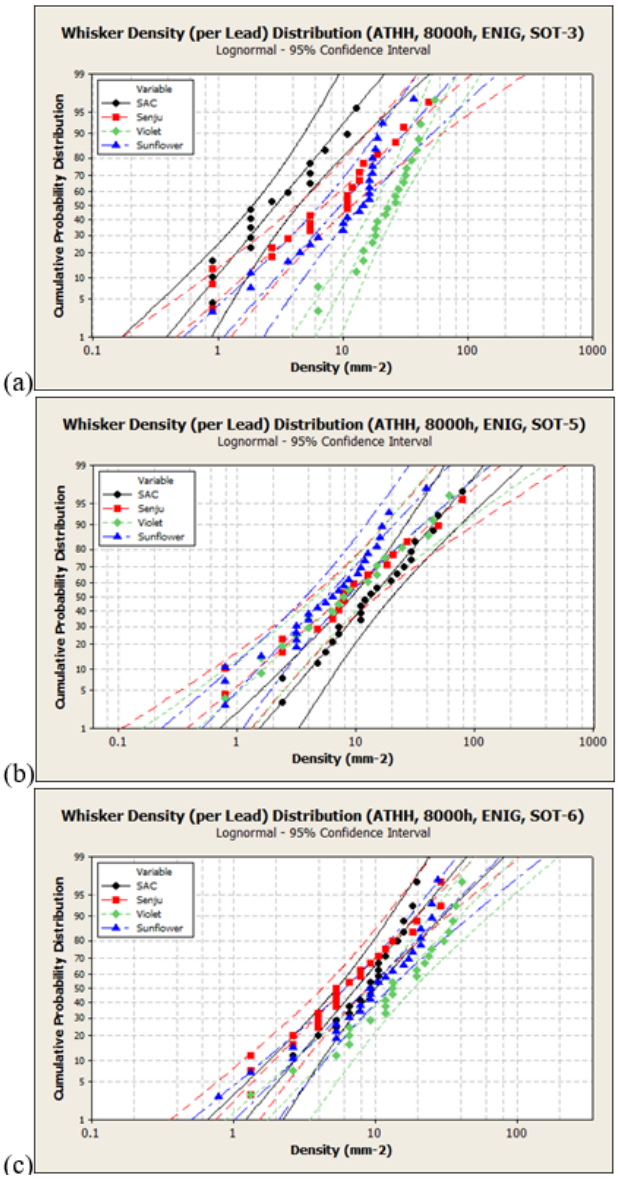

Figure 12: Lognormal probability plots of whisker density on a per lead basis, for ENIG-finished assemblies. SOT-3 (a); SOT-5 (b); SOT-6 (c).

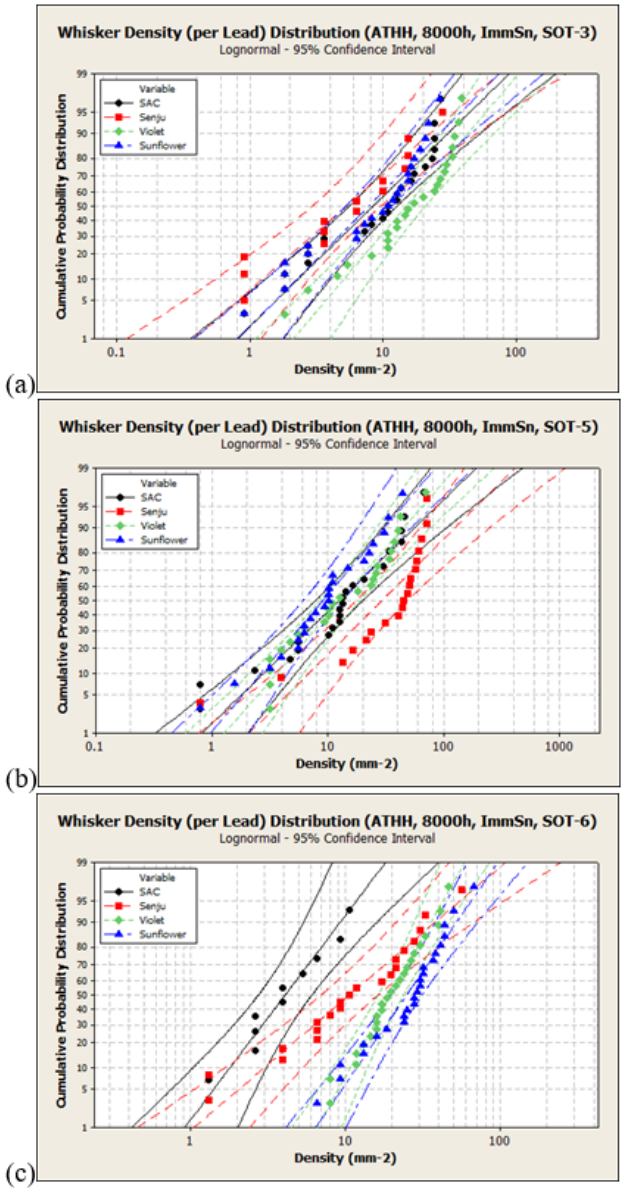

Figure 13: Lognormal probability plots of whisker density on a per lead basis, for ImmSn-finished

Table 4: Lognormal Distribution Parameters (ENIG)

Part	Alloy	N	Location	Scale	AD
SOT-3	SAC 305	16	1.06	0.86	0.498
	Senju	20	1.96	1.17	0.501
	Violet	22	3.10	0.56	0.423
	Sunflower	23	2.26	0.93	1.439
SOT-5	SAC 305	22	2.60	0.94	0.180
	Senju	16	2.06	1.31	0.219
	Violet	19	2.06	1.21	0.144
	Sunflower	25	1.72	1.03	0.429
SOT-6	SAC 305	23	1.99	0.77	0.784
	Senju	23	1.82	0.91	0.252
	Violet	23	2.57	0.87	0.484
	Sunflower	24	2.28	0.80	0.477

Table 5: Lognormal Distribution Parameters (ImmSn)

Part	Alloy	N	Location	Scale	AD
SOT-3	SAC 305	23	2.13	1.01	0.924
	Senju	14	1.67	1.13	0.528
	Violet	24	2.70	0.84	0.733
	Sunflower	23	2.05	0.97	1.002
SOT-5	SAC 305	24	2.53	1.17	0.754
	Senju	19	3.38	1.13	1.800
	Violet	24	2.55	0.99	0.600
	Sunflower	23	2.20	0.96	0.344
SOT-6	SAC 305	10	1.40	0.64	0.243
	Senju	21	2.36	0.99	0.375
	Violet	24	2.98	0.47	0.154
	Sunflower	24	3.21	0.58	0.599

Overall, the density data demonstrates varying degrees of fit to the lognormal distribution. Several observations that can be made about these probability plots are as follows:

• Generally, a wider spread in densities can be seen on Cu194 leads (SOT-5) than Alloy 42 leads. Both lead materials show about the same wellness of fit to the lognormal distribution, overall.
• Overall, ENIG shows a slightly wider spread in density (across all parts/alloys) and fits the lognormal distribution slightly better than ImmSn.
• Several data sets show extremely poor fit to the lognormal distribution (AD > 1). These are ENIG, SOT-3, Sunflower (Figure 12a); ImmSn, SOT-3, Sunflower (Figure 13a); and ImmSn, SOT-5, Senju (Figure 13b). These have AD values of 1.439, 1.002, and 1.800, respectively. The latter shows high average whisker density (Figure 11) – this may be caused by the uncharacteristically high number of leads with high whisker density.
• No clear trends can be seen with respect to alloy, considering these distributions.

Whisker Diameter and Angle

Boxplots showing the distribution of average whisker diameter for the different alloys and board finishes is given in Figure 14. If a whisker diameter changed over its length, the average of the minimum and maximum diameter was reported. It is observed that diameter is not largely dependent on alloy, particularly for ImmSn, though for both finishes, the median whisker diameter is slightly larger on the alloy with higher Bi content (Violet and Sunflower). Overall, for both ENIG and ImmSn, the diameter distributions do not appear to be statistically significant between alloys. The overall average diameter for the ENIG board finish is 2.6 microns and for the ImmSn is 3.5 microns.

Scatter plots showing the relationship between whisker length and diameter are given in Figure 15. Generally, very little correlation is observed, save ENIG-Senju and ImmSn-SAC. The longest whiskers were between two and eight microns in diameter.

The count of whisker growth angles is summarized in Figure 16. For the ImmSn finish, the majority of the whiskers had an angle of zero degrees, which means that the growth angle was relatively shallow (e.g. less than ~20-25 degrees as defined in Figure 5).

The complete set of data from the whisker inspection of the SOT assemblies after 12000 hours is given in the appendices of the original version of this paper, published at the 2018 SMTA ICEET conference.

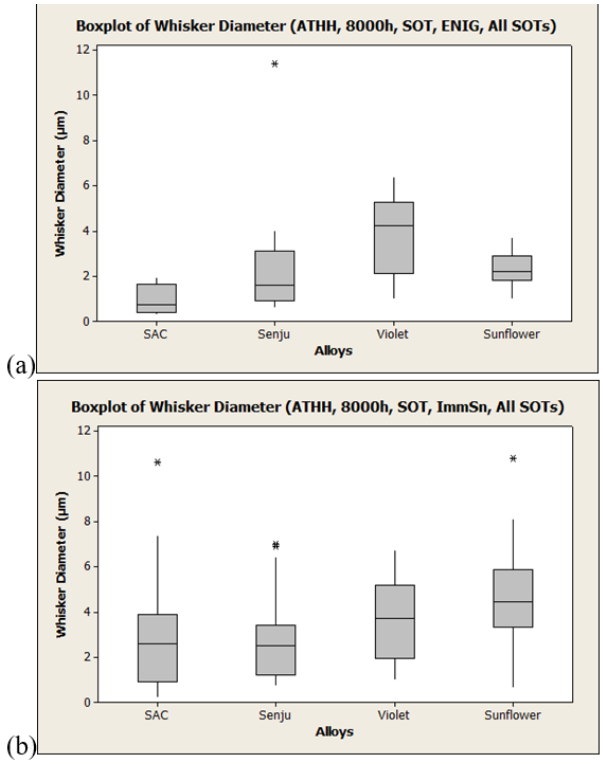

Figure 14: Statistical distribution of measured whisker diameters on ENIG (a) and ImmSn (b) finished boards, by alloy

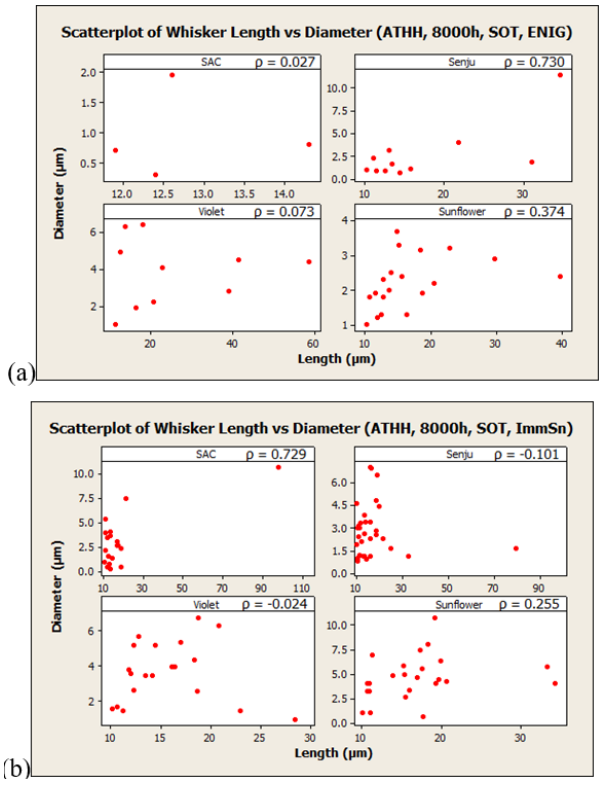

Figure 15: Whisker diameter versus length for the SAC, Senju, Sunflower and Violet alloys, with correlation coefficients ρ (a) ENIG and (b) ImmSn.

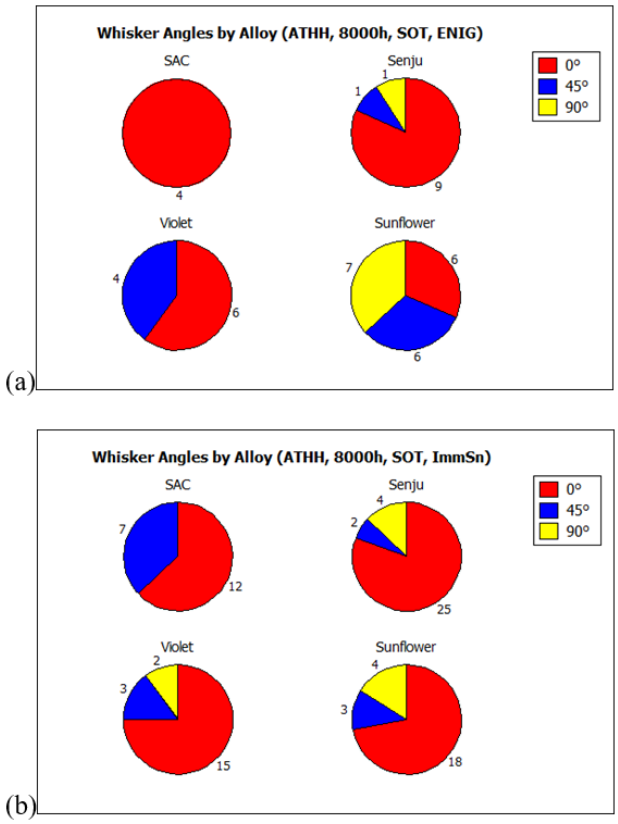

Figure 16: Count of whisker angle incidence for the SAC, Senju, Sunflower and Violet alloys; (a) ENIG and (b) ImmSn.

DISCUSSION

Role of Bi in Whiskering

After reflow, Bi forms a supersaturated solid solution with Sn. Over time, Bi will precipitate out of solution, forming small particles. The solid solubility of Bi in Sn is roughly 2 wt%; the higher the Bi content in the alloy, the greater volume fraction of Bi precipitates. In addition, the Bi precipitates become more homogenously distributed through the alloy over time [14], likely due to continuous dissolution and re-precipitation at the exposure temperature (25°C). Migration of Bi precipitates from the interdendritic spaces results in loss of dendritic structure of the primary Sn. In addition, larger Bi precipitates will not undergo dissolution/re-precipitation; rather they will remain out of solution and undergo Ostwald ripening (Dissolution of small grains in favor of growing larger grains) as some Bi migrates to the phase boundaries between the large particles and Sn matrix (Figure 17).

In addition, Bi precipitation induces the recrystallization of the Sn matrix [15] into a homogeneous, equiaxed grain structure (Figure 18). This is likely a result of density and crystal structure mismatch between the Sn and Bi phases (Table 6) – as Sn is softer and more ductile than Bi, it will experience stress due this mismatch. Recrystallization is the result of the Sn matrix relieving this stress. It is believed that whisker nucleation and growth is analogous to recrystallization – while grain size in the bulk is restricted by neighboring grains, the free surface provides an opportunity for unhindered grain growth which results in a whisker. In SAC 305, whiskers are generally longer and sparser because the stress is higher in more localized regions. Adding Bi to the alloy causes a more distributed stress condition in the joint, resulting in more nucleation sites for whiskers. These whiskers, however, are substantially shorter and less of a reliability risk.

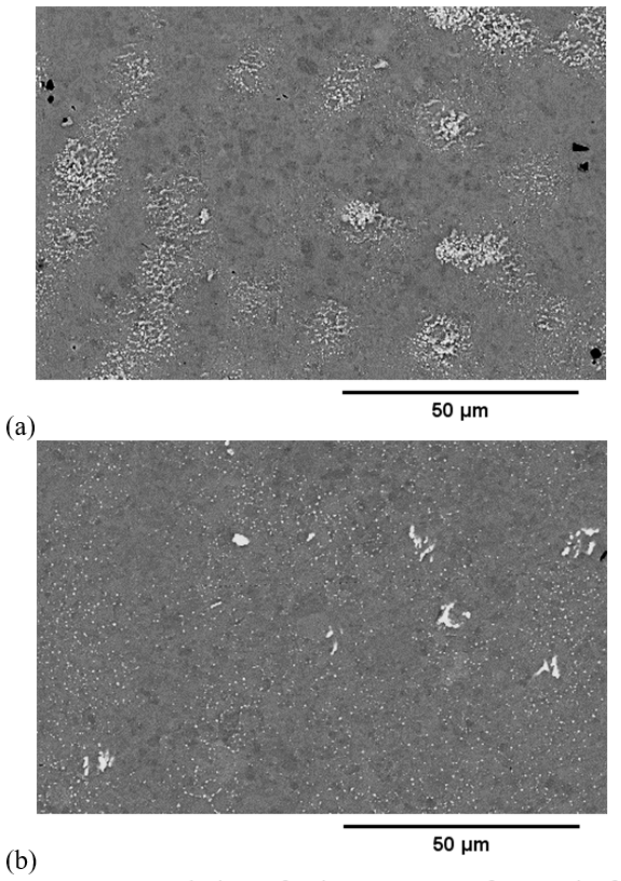

Figure 17: Evolution of microstructure of Sn-5Bi after aging at room temperature [14]; (a) As-cast and (b) after 168 days. With aging time, Bi precipitates become more evenly distributed and some precipitates undergo Ostwald ripening.

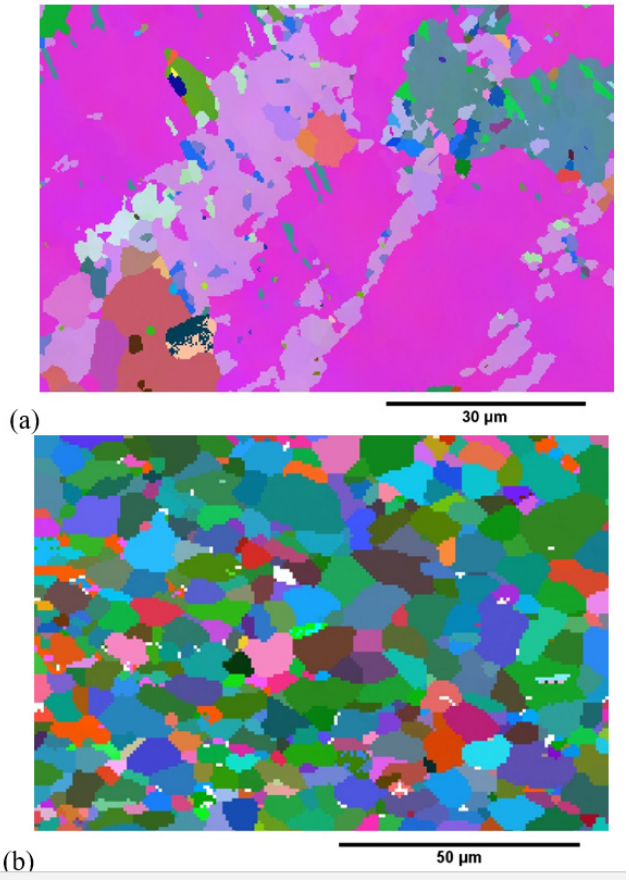

Figure 18: Recrystallization of Violet after aging [15]; (a) As cast and (b) after aging at 125°C for 100 hours.

Table 6: Density and crystal structure data for Sn and Bi.

Metal	Density (g/cm^3)	Crystal Structure
Sn	7.27	Body-centered tetragonal
Bi	9.78	Rhombohedral

Role of Bi in Corrosion

The addition of Bi to the alloy may also exacerbate corrosion, which would result in an increase in whiskers. This would be prevalent in alloys with substantial Bi precipitation (Violet and Sunflower). Examination of the galvanic series (Table 7) indicates that Bi is more noble than Sn [16] and thus in a Sn-Bi couple, the Sn will preferentially corrode (as observed in Figure 19). The galvanic cell analysis is as follows:

#	Half Reactions	Standard Half Cell Potential (V)
1	$Bi_2O_3 + 3H_2O + 6e^- \rightarrow 2Bi + 6OH^-$	-0.46V
2	$SnO_2 + 2H_2O + 4e^- \rightarrow Sn + 4OH^-$	-0.945V
3	$Cu_2O + H_2O + 2e^- \rightarrow 2Cu + 2OH^-$	-0.36V

Rearranging to combine Reactions 1 and 2 into Reaction 4, and 2 and 3 into Reaction 5:

#	Reaction	Standard Cell Potential (V)
4	2Bi2O3 + 3Sn → 4Bi + 3SnO2	+0.485V
5	2Cu2O + Sn → 4Cu + SnO2	+0.585V

Table 7: Abridged galvanic series of metals in sea water [16]. The galvanic potential for Au was not included; the value for Pt is given as it behaves comparably to Au.

Metal	Median Potential (V) (SCE Reference)
Gold	+0.295
Copper	-0.141
Nickel	-0.172
Bismuth	-0.248
Tin	-0.671

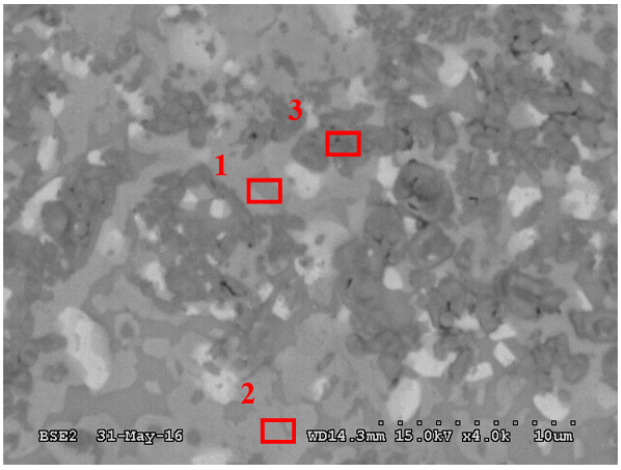

Figure 19: 4000h inspection showing corrosion between Sn and Bi on a cleaned SOT6 lead with Sunflower on an ENIG finished pad (4000x magnification). EDX locations are labelled; the bright white particles are Bi.

The net standard cell potentials are positive, which suggests that the reactions will proceed to the right, and Sn will preferentially oxidize in a couple with either Bi or Cu. It supports the SEM/EDX results (Table 8) where corrosion of Sn occurred around Bi precipitates, and the lack of Bi in the outer oxide layer of the corroded whisker (Bi is rejected from the growing oxide layer into the core of the whisker). Note if SnO instead of SnO_2 (V = -0.10V) is used, the net cell potential is negative (-0.36V), which would suggest that Bi_2O_3 and Sn will coexist rather than SnO and Bi. Since this was not observed in the current EDX data, it is more likely that SnO_2 is taking part (or predominant) in this galvanic cell.

In addition, phase boundaries (e.g. between Sn and Bi) are more active than bulk material and are more susceptible to corrosion.

Finally, the recrystallization of the alloy induced by Bi precipitation causes an increase in Sn grain boundaries, which are also high energy boundaries that are more susceptible to corrosion.

Table 8: Detailed EDX spectra for Figure 19.

Element	pt 1	pt 2	pt 3
C	7.34	6.40	7.80
N	5.26	4.62	3.28
O	6.31	5.11	5.11
Si	0.00	0.00	1.21
Ni	0.00	1.02	8.89
Cu	0.00	0.00	13.33
Sn	76.15	69.81	54.47
Au	1.39	9.48	4.46
Bi	3.55	3.56	1.45

Effect of Au in Corrosion on ENIG finish

The galvanic series suggests that Au is more noble than all other species in the joint [16]. This fact, in addition to the Sn-Bi galvanic effect and increase in grain and phase boundary content in Bi-bearing alloys, may explain the increased whiskering on ENIG at L2 and L5 shown in Figure 9. These locations are close to the pad and thus likely richest in Au. Significantly fewer whiskers were seen in these locations for SAC, likely because the whisker-inducing effects of Bi were not present.

SUMMARY AND CONCLUSIONS

Several key takeaways from the statistical results of this study are as follows:

- On cleaned assemblies, generally a higher proportion of parts/leads show whiskers as the Bi content is increased.
- On ImmSn, whiskers were generally shorter and more consistent on alloys with high Bi content (Violet and Sunflower), however the opposite is observed for ENIG.
- On cleaned assemblies and on contaminated ImmSn assemblies, whisker growth was restricted to regions with thin solder coverage, such as L1, L3 and L4.
- However for contaminated ENIG assemblies, while showing fewer whiskers than ImmSn, substantially more whiskers were observed on locations close to the pad (L2 and L5). This may be caused by an exacerbation of corrosion related to the nobility differences between the various species present at these regions (such as gold from the surface finish).
- Whisker diameter is not strongly correlated with whisker length or alloy type, however diameter is slightly larger for the higher-Bi alloys (Violet and Sunflower).

From a practical perspective, it is challenging to keep an initially clean assembly from getting incidental contamination that can promote whisker growth during the product life cycle. The typical practice of conformal coating a product helps reduce the risk of incidental contamination by providing an added barrier between the environment and the termination. It is for this reason that full coverage of conformal coating is desired for whisker mitigation.

The utilization of clean boards permits evaluation of the alloy impact on whisker formation. Contamination and corrosion may mask the effects of alloy additions and other growth mechanisms. In longer tests, where corrosion results in whiskers falling off or possibly becoming consumed by the corrosion products, it can also influence whisker density and length results.

It is important when studying whisker growth of solder joints that all the material interaction be considered. For ImmSn, there were more whiskers on the Bi-bearing alloys, but they were shorter in length and more kinked/curved than the SAC305 terminations. This is believed to represent a more even distribution of stress due to a greater number of small Sn grains as compared to the SAC alloy. However the opposite is observed for ENIG, suggesting that consideration of multiple mechanisms contributing to whiskering must be considered. This will be done in the third paper in this series.

FUTURE WORK

One follow-up paper is planned which supplements the work shown in this paper and in Part 1. In that paper (Part 3), more analytical work, including cross-section and EDX, of interesting features will be provided. In addition, screening inspection results from QFP and BGA boards will be shown, and the results from a detailed inspection of the latter will be included in a further future publication.

Further whisker mechanisms will be proposed and discussed, notably with respect to the role of Bi and Au in the corrosion of solder joints. In addition, an expansion to the previously discussed whisker 'sweet spot' concept, considering the effects of Bi on the stress state in solder joints and subsequent response of the microstructure, will be considered.

ACKNOWLDEGEMENTS

The authors would like to thank the Canadian ReMAP program, Russell Brush, Celestica, for the environmental testing, and Ivan Tan, Celestica, for the assembly.

REFERENCES

[1] GEIA-STD-0005-2, Standard for Mitigating the Effects of Tin Whiskers in Aerospace and High Performance Electronic Systems, SAE International, Warrendale, PA.

[2] P.T. Vianco, M.K. Neilsen, J.A. Rejent, and R.P. Grant, Validation of the Dynamic Recrystallization (DRX) Mechanism for Whisker and Hillock Growth on Sn Thin Films, Journal of Electronic Materials, Vol. 44, No. 10, 2015, pp. 4012 – 4034.

[3] G.T. Galyon, Annotated Tin Whisker Bibliography and Anthology, IEEE Trans. Packag. Manuf. Vol. 28, No. 1, January 2005, pp. 94-122.

[4] J. Nielsen and T. Woodrow, The Role of Trace Elements in Tin Whisker Growth, Project WP1751 Final Report for the Strategic Environmental Research and Development Projects (SERDP), September 22, 2013.

[5] I. Yanada, "Electroplating of Lead-Free Solder Alloys Composed of Sn-Bi and Sn-Ag, Proc. Of the IPC Printed Circuits Expo, Long Beach USA: pp. S11-2 to S11-2-7, April 1998.

[6] S. Meschter, P. Snugovsky, Z. Bagheri, E. Kosiba, M. Romansky, J. Kennedy, L. Snugovsky, and D. Perovic, Whisker Formation on SAC305 Soldered Assemblies, JOM, vol. 66 no. 11, pp. 2320-2333, Nov. 2014 (DOI) 10.1007/s11837-014-1183-9, available on line at

http://www.springer.com/home?SGWID=0-0-1003-0-0&aqId=2737780&download=1&checkval=c6d6cb73aec6cca572a5b064f23677b9

[7] P. Snugovsky, S. Meschter, Z. Bagheri, E. Kosiba, M. Romansky, and J. Kennedy, Whisker Formation Induced by Component and Assembly Ionic Contamination, Journal of Electronic Materials, February 2012, Volume 41, Issue 2, pp 204-223, available for download at http://link.springer.com/content/pdf/10.1007%2Fs11664-011-1808-5.pdf

[8] S. Meschter, P. Snugovsky, J. Kennedy, and Z. Bagheri , ReMAP Materials Project M2: High Temperature High Humidity Corrosion and Tin Whisker Evaluation of Bi containing Lead-free Alloys, International Conference on Soldering and Reliability, (ICSR) Toronto, Canada, May 10-11, 2016

[9] S. Meschter, Tin Whisker Testing and Modeling, Project WP1753 Final Report, U.S. DoD, EPA, DOE Strategic Environmental Research Programs (SERDP), November 2015, available for download at: https://www.serdp-estcp.org/Program-Areas/Weapons-Systems-and-Platforms/Lead-Free-Electronics/WP-1753

[10] S. Meschter, E. Ekstrom, P. Snugovsky, J. Kennedy, Z. Bagheri, and E. Kosiba, Strategic Environmental Research and Development Program (SERDP) Tin Whisker Testing and Modeling: Long Term Low Temperature High Humidity Testing, International Conference on Soldering and Reliability (ICSR), Toronto, Ontario, Canada; May 19-21, 2015.

[11] JESD201 Environmental Acceptance Requirements for Tin Whisker Susceptibility of Tin and Tin Alloy Surface Finishes, JEDEC Solid State Technology Association, Arlington, VA 2006

[12] S. Meschter, P. Snugovsky, J. Kennedy, Z. Bagheri, and E. Kosiba, Tin Whisker Testing: Low Stress Conditions, SMTA International Conference on Solder Reliability, Toronto, Ontario, Canada, 2012

[13] JESD22A121A Test method for measuring whisker growth on tin and tin alloy surface finishes, JEDEC Solid State Technology Association, Arlington, VA 2000.

[14] A. Delhaise, D. Perovic, P. Snugovsky, "The Effects of Aging on the Microstructure and Mechanical Properties of Bi-Containing Sn-Rich Alloys," J. Surface Mount Technology, 30, 2 (2017), pp. 21-27

[15] A. Delhaise, P. Snugovsky, I. Matijevic, J. Kennedy, M. Romansky, D. Hillman, D. Adams, S. Meschter, J. Juarez, M. Kammer, I. Straznicky, L. Snugovsky, D. Perovic, "Thermal Preconditioning, Microstructure Restoration, and Property Improvement in Bi-Containing Solder Alloys," J. Surface Mount Technology, 31, 1 (2018), pp. 33-42

[16] J.A. Smith, P.E. Groover, T.J. Lennox Jr., M.H. Peterson, "The Electrochemical Potential of High Purity Metals in Seawater," Naval Research Laboratory Memorandum Report 2187 (November 1970)

BIOGRAPHIES

André Delhaise is a metallurgist at Celestica, Inc., and is actively involved in several projects in association with the Refined Manufacturing Acceleration Process (ReMAP), which is a Canadian-led consortium of academic and industry partners focused on the commercialization of novel manufacturing technologies and processes. He is also involved in the iNEMI 3rd generation Pb-free alloy characterization effort as well as the Pb-free Risk Management (PERM) group. André is also currently a PhD Candidate in the Department of Materials Science & Engineering at the University of Toronto, specializing in the metallurgy of bismuth-containing lead-free solders, under the supervision of Dr. Doug D. Perovic. He holds a Bachelor of Applied Science (BASc) degree from the same department, obtained in 2013. André was awarded the 'Best of Proceedings' award at the SMTA International Conference in 2017, and has published several papers in refereed journals such as the Journal of Electronic Materials (JEM).

Dr. Stephan Meschter has over 30 years of experience in advanced packaging, failure analysis, and reliability testing of electronic assemblies at BAE Systems Electronic Systems in Endicott, NY. He has designed and evaluated electronic assemblies for power, flight and jet engine control systems used in spacecraft, aircraft and ground vehicles. Starting in 2004, Stephan began evaluating the commercial lead-free materials transition impact to high-reliability, high-performance aerospace and defense electronic systems. He was a member of the 2009 U.S. DoD Lead-free Electronics Manhattan Project team that published a set of best practices to mitigate the risks associated with Lead(Pb)-free electronics usage in high performance DoD systems. Since 2010, Stephan has worked with SERDP on lead-free tin whisker formation research and short circuit risk mitigation using enhanced polymer conformal coatings. He earned a bachelor's in mechanical engineering from the University of Hartford in Hartford CT in 1984, and he holds both a master's degree (1987) and a doctoral

degree (2001) in Mechanical Engineering from the State University of New York in Binghamton, NY. Stephan currently participates in the IPC Lead(Pb)-free Electronics Risk Management (IPC-PERM) Council and is currently supporting revision of several SAE GEIA Lead-free Aerospace and Defense risk management standards.

Polina Snugovsky recently served as Principal Engineer - Chief Metallurgist at Celestica. Polina was an invited subject matter expert participant in the 2009 Pb-free Manhattan Project tasked with the risk assessment of Pb-free electronics in Aerospace and DoD applications. Polina was an active participant in the Pbfree electronics in aerospace project group (AIA PERM) - American Institute of Aeronautics. She was the principal investigator of two U.S. DoD Strategic Environmental Research and Development Projects (SERDP) that are examining corrosion induced whisker growth and manufacturing mitigation. She has also actively participated in NASA DoD projects. Dr. Snugovsky graduated from the State Metallurgical Academy of Ukraine and received her Ph.D. in Metallurgy, and subsequently in 1985 she earned the higher level Doctoral degree in Metallurgy and Material Science. Before she joined Celestica in 1996, she was a full professor in the department of physical metallurgy of the State Metallurgical Academy of Ukraine. She has published over 160 papers and patented new materials and processes. Polina holds several Outstanding Technical Achievement Awards, including two from Celestica and received Best International Conference Papers awards at SMTA2006, APEX2007, APEX2009, APEX2010, APEX2013 and APEX2014. In 2012 she received SMTA Member of Technical Distinction Award.

Jeff Kennedy is currently the Strategy and Business Development Manager at ZESTRON Americas. Prior to that he directed Celestica's advanced technology strategy and development initiatives, including the design and implementation of technology roadmaps for the Industrial and A&D sectors. Jeff has more than 30 years of experience in system integration, process development, PWB fabrication, and packaging in the microelectronics industry. He has engineering and management experience working within mainframe computer industry, microcircuit wire bonding and flip chip, PWB fabrication and laminate packaging substrates, and the last 16 years in contract electronics assembly. Jeff is a past President of SMTA and is an active member of both IPC & IMAPS.

INVESTIGATION OF SOLDER JOINT ENCAPSULANT MATERIALS FOR DEFECT MITIGATION

S.Y. Teng[1*], C. Guirguis[1], G. Ramakrishna[1] and H. Ly[2]
[1]Cisco Systems, Inc. and [2]Jabil Circuits, Inc.

ABSTRACT

As next-generation networking equipment continue to push the trends of higher signal speeds and increased functional density, the need for advanced PCB structures, such as Via-in-Pad Plated Over (VIPPO) and backdrill, and high-speed memory is becoming more mainstream across product platforms. Furthermore, as these high-speed memory technologies are being driven by consumer applications, the form factor and interconnect pitches continue to shrink to meet the demands of the mobile device market. The use of these advanced PCB structures, like VIPPO and VIPPO with backdrill, within the BGA footprints, particularly for the fine pitch patterns, have been found to result in BGA solder separation defects at the bulk solder to IMC interface upon a 2nd reflow, e.g. during top-side reflow for bottom-side components or during rework of an adjacent BGA.1 This type of solder separation occurs during reflow and is associated with out-of-plane CTE mismatch underneath adjacent BGA pads as well as a differential in the time to reach liquidus for adjacent BGA solder joints due to disparities in thermal conductivity of those areas underneath the adjacent BGAs. It is not a non-wet or solder fracture in that there is a properly formed intermetallic compound (IMC) layer between the Cu pad and the solder and the separation occurs between the bulk solder and the IMC and is not initiated at a crack. In some cases, this solder separation failure mode has also been identified with buried vias under the BGA pad. 2.3 Additionally, small memory components have been experiencing high occurrences of head-in-pillow (HIP) defects even though the overall package warpage over the reflow profile is < ~3mils.

This paper will therefore focus on the mitigation of these solder joint defects resulting from SMT assembly with the use of solder joint encapsulant materials to provide enhanced adhesion strength for the solder joints. Leveraging existing test vehicles that are known to induce the aforementioned solder joint defects, two different solder joint encapsulant or epoxy flux materials are evaluated in terms of the application process, assembly integrity and compatibility with standard SAC305 production solder paste materials and SMT processes.

Key words: BGA solder joint defects, Head-in-Pillow (HIP), BGA solder separation, epoxy flux, solder joint encapsulant, SMT assembly, Via-in-pad plated over (VIPPO), solder hot tear, solder joint reliability, ATC testing

INTRODUCTION

With the trend of increasing signal speeds, board functional density and PCB layer count/thickness, PCB structures and designs are becoming more complex, and are resulting in new or unique solder joint defects during assembly. As discussed previously, increased occurrences of the solder separation defect have resulted with the introduction of the mixed VIPPO BGA footprint designs within the PCB. Moreover, the occurrence of HIP defects on small body BGA packages with very low package warpage over the reflow profile has emerged as well. Typically, these HIP defects are attributed to PBGA packages with high package warpage characteristics over the reflow profile. These types of HIP defects can be addressed by either modifying the package design and/or modifying the SMT reflow process. In order to optimize the package design for improved warpage behavior, the package design can be rigidized or modified to minimize the effects of the CTE mismatch within the package. For instance, using a stiffener ring with heat spreader instead of a top-hat lid design and employing a thick core (e.g. 800um or 1.2mm core thickness) substrate will increase the stiffness of the package and help to control the magnitude of the package warpage experienced over the reflow profile. Additionally, optimizing the underfill material properties to reduce the chip-to-package interaction (e.g. having a lower Tg) can also help to minimize the resulting package warpage. In terms of the SMT process, the reflow profile and process can also be optimized to mitigate HIP defects by reducing solder oxidation, minimizing flux exhaustion prior to reflow and allowing for more time during reflow for the solder ball and paste to coalesce. This can be achieved with the use of nitrogen to create an inert environment during SMT, reducing the soak time and increasing the time above liquidus. Finally, these HIP defects can also be mitigated by controlling the printed solder volume on the BGA pads as a function of the location and the package warpage in that area. However, for these new HIP defects that are not dependent on the package warpage, these SMT process parameters may not be sufficient to mitigate the defects and alternative mitigation strategies become necessary.

The primary objective for this evaluation is, therefore, to assess the effectiveness of two different solder joint encapsulant or epoxy flux materials in terms of their ability to mitigate both the solder separation defects associated with the use of VIPPO within the PCB BGA footprint as well as the HIP defects for small BGAs with < 3 mils warpage. These encapsulant materials being investigated in this study provide an attractive alternative to underfill materials as they can be assembled in-line without the need for additional specialized equipment. Furthermore, these materials can be cured during reflow, and hence, do not require additional processing steps and do not significantly increase cycle times.

*Currently employed at Google

Existing test vehicles that have exhibited both of these defects will be employed for this study. These test vehicles will be assembled with each of the solder joint encapsulant or epoxy flux materials included within this study. Ease and performance of the application process for each of the materials will be evaluated. Additionally, inspection and physical analysis will be used to assess the solder joint integrity to understand the effectiveness of these materials for defect mitigation. Finally, these materials will also be evaluated in terms of their compatibility with existing production materials and processes.

EVALUATION PLAN

Two existing test vehicle designs have been implemented for this investigation. These test vehicles have previously been demonstrated to induce both the solder separation defect with a mixed VIPPO/non-VIPPO BGA footprint as well as the HIP defect for small BGA packages with very small package warpage over the reflow temperature excursion. In addition, two different solder joint encapsulant materials are targeted for this study, both of which employ a similar application process that can be incorporated in-line with conventional SMT equipment. Both encapsulant material manufacturers cited their materials to be compatible with standard SAC305 solder paste systems.

A dip process was implemented within the pick and place equipment (after the solder printing process) in order to apply the encapsulant materials to the BGA balls of each component, similar to a flux dip process. For this process, the pick and place equipment uses a dip tray filled with the encapsulant material. As illustrated in Figure 1, during pick and place, the component was picked up, dipped into the encapsulant material and then placed onto the printed solder of the PCB pads. The amount of encapsulant material applied to the BGAs was controlled by the depth of the dip tray. For these evaluations, a dip depth of 85% of the BGA diameter was used to ensure adequate coverage of the encapsulant up to the BGA package pad interface. Dip dwell times ranged from 0.3 to 1 sec, depending on the encapsulant material and BGA diameter/pitch. These encapsulant materials were then cured during the SMT reflow process. Therefore, there are no additional handling or process steps required for implementation of these encapsulant materials. Both of these materials are also advertised to be reworkable with standard BGA rework processes, but that is beyond the scope of this investigation.

For this investigation, each of the test vehicles includes a set of control boards, a set of boards with parts dipped in encapsulant A and a set of boards with parts dipped in encapsulant B. Each of these boards is evaluated after SMT assembly via x-ray inspection techniques with 1 board of each set also subject to physical analysis. The remaining boards are then subject to a 2nd reflow in order to simulate a secondary top-side reflow process. This was conducted to attempt to induce the solder separation defect. Again, each of the boards was inspected via x-ray with 1 board of each group subject to physical analysis. Finally, the remaining boards were submitted to accelerated temperature cycle (ATC) testing per IPC-9701, using the 0°C to 100°C temperature cycle range.

Figure 1: Encapsulant Assembly Process

For the control boards, dye and pry techniques in addition to x-sectioning were utilized to validate the inspection results. However, with the encapsulant materials, only x-sectioning is utilized for physical analysis. Since the encapsulant material may inhibit accurate results regarding the solder joint integrity with the use of a dye and pry technique, this was not used for physical analysis of the boards having the encapsulant materials.

TEST VEHICLE

Test vehicle 1 (TV1), shown in Figure 2, was designed to investigate the influence of various design parameters on the solder joint integrity in a mixed VIPPO and non-VIPPO BGA footprint within the PCB for a given set of controlled PCB factors such as PCB thickness (125 mils), material (Megtron 6) and number of stack-up layers (16). This design used the footprint for DDR4 BGA components (13.3 x. 7.5 mm sq., 0.8mm pitch) for this evaluation.

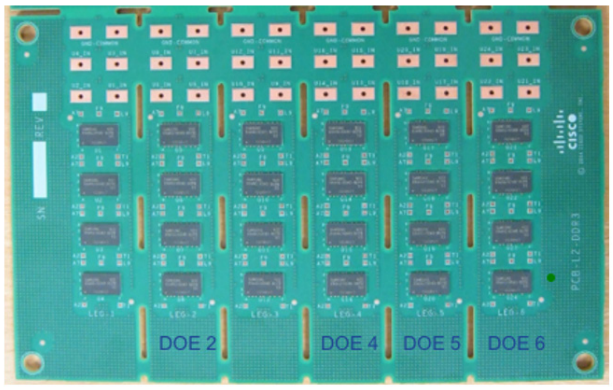

Figure 2: Test Vehicle 1 (TV1)

For TV1 shown above, the package footprint is exhibited in Figure 3 below. Only the locations marked as DOE2, DOE4, DOE5 and DOE6 are populated for the purposes of this evaluation, as these are the locations having a footprint with the PCB design attributes known to induce both of the solder joint assembly defects targeted for this study.

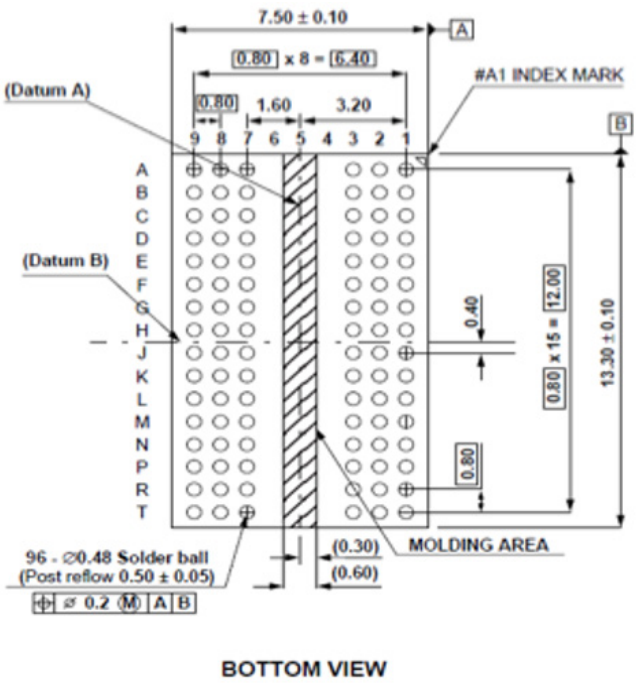

Figure 3: Package Footprint on Test Vehicle 1 (units in mm)

Test vehicle 2 (TV2), shown in Figure 4, includes a variety of fine pitch BGA component sizes and BGA pitches, again having mixed VIPPO and non-VIPPO BGA footprints. This board design includes BGA body sizes, ranging from 10x10 mm sq. up to 37x37 mm sq., and BGA pitches, ranging from 0.7mm to 1.0 mm. Again, the same set of controlled PCB factors as defined in TV1 for thickness, PCB material and stack-up are also employed. Neither test vehicle includes any components on the bottom-side.

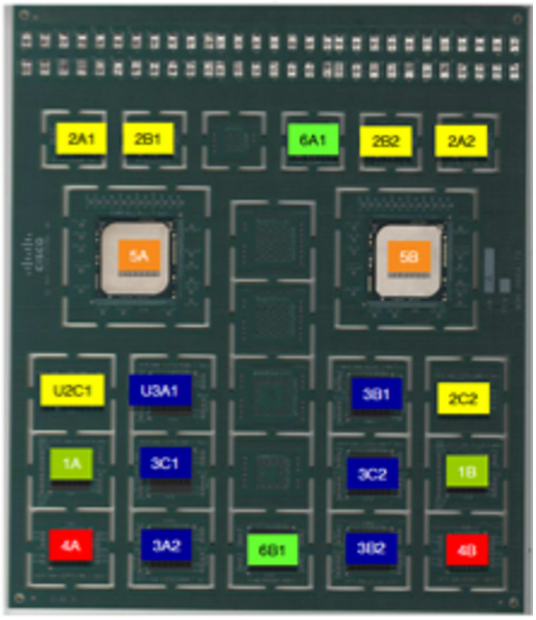

Figure 4: Test Vehicle 2

ASSEMBLY PROCESS

In order to understand the compatibility of these solder joint encapsulant materials with existing standard SMT assembly materials and processes, both test vehicles are assembled with two different production solder pastes and conventional production SMT equipment is used, including solder paste printing, pick and place and reflow. Subsequently, x-ray inspection is performed although digital x-ray tomosynthesis capabilities were not available for this study.

Each test vehicle is assembled and subsequently put through a secondary reflow in order to simulate both a secondary SMT attach process, followed by inspection and physical analysis to validate the solder joint integrity after each reflow. Reflow profiles for both test vehicles are shown in Figures 5a and 5b below. The printed circuit assembly equipment, process parameters, tooling (e.g. stencil design and technology), and assembly materials (e.g. solder paste) utilized for these builds are consistent with standard production processes in order to minimize the number of variables introduced in this study. However, as this assembly was performed in a development lab rather than a production floor, access to the 5DX or equivalent digital x-ray tomosynthesis inspection equipment was not available.

Figure 5a: DDR4 TV Reflow Profile

Figure 5b: Fine Pitch TV Reflow Profile

RESULTS

Assembly

The assembly performance of two solder joint encapsulant materials were compared with control boards having no solder joint encapsulant material for two different test vehicle designs, a DDR4 test board and a fine pitch test board.

As expected, the DDR4 test vehicle, which used a component package previously known to result in HIP defects, was found to

exhibit numerous HIP defects after the initial SMT reflow on the control boards. These HIP defects occurred similarly with both solder pastes and, after the 2nd reflow, these HIP defects were mostly 'healed'. During the secondary reflow, when there is a forced constraint of the package due to the previously formed solder joints, any movement of the package is restricted prior to reflow so that these HIP joints are able to properly coalesce and 'heal' during reflow. After the 2nd reflow, there were, however, significant solder separation defects present on the control boards, again, regardless of solder paste, as shown in Figure 6. Both solder joint encapsulant materials were found to mitigate the solder separation defects on the DDR4 test vehicle as shown in Figure 7, but only the solder joint encapsulant material A, however, was able to mitigate the HIP defects. Extensive solder voiding was also identified with the solder joint encapsulant material B and is illustrated in Figure 9. This voiding was considered to be within IPC workmanship standards, but was marginal in some cases and would require additional process optimization. However, for the purposes of this study, further investigation of this voiding phenomenon was not pursued. The solder joint encapsulant B material also exhibited solder bridging defects as shown in Figure 9, possibly due to inconsistent coverage or voiding of the encapsulant material leading to solder extrusion, and there was significant solder balling both within the BGA array as well as around the periphery of the package, as seen in Figure 8.

For the Fine Pitch test vehicle, the control boards and boards using the solder joint encapsulant B material exhibited solder separation defects after the 2nd reflow, as illustrated in Figure 10. This occurred primarily with one of the solder pastes. Moreover, the boards using the solder joint encapsulant B material again exhibited extensive solder voiding, solder bridging and solder balling as seen in Figure 11. The boards using the solder joint encapsulant A material, however, were shown to mitigate the solder separation defect. These boards did show pronounced solder voiding, as seen in Figure 12, which was within IPC workmanship standards, but, again, marginal in some cases and would require further optimization. Additionally, for the largest package size, the 37.5 mm sq. FCBGA, the solder joint encapsulant A material was found to be uncured underneath the center of the package, even after 2 reflows. Further investigation by the material manufacturer has been pursued to address this issue. Similar results were exhibited with both solder pastes.

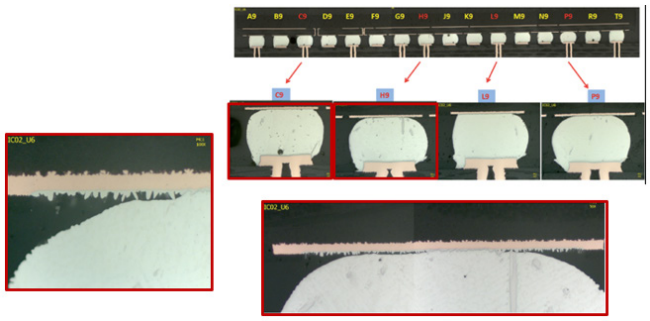

Figure 6: Solder Separation on DDR4 Control Boards

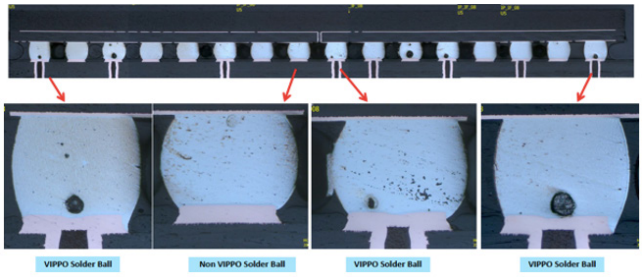

Figure 7: DDR4 TV Assembly Results with Solder Joint Encapsulant Material A

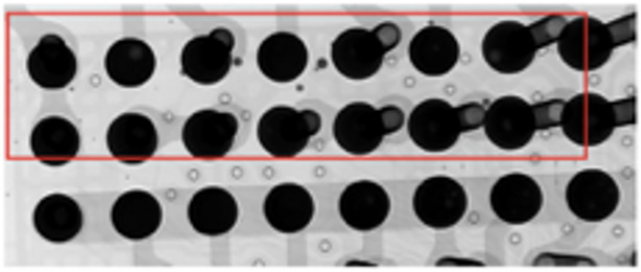

Figure 8: Solder Balling with Solder Joint Encapsulant Material B on DDR4 TV

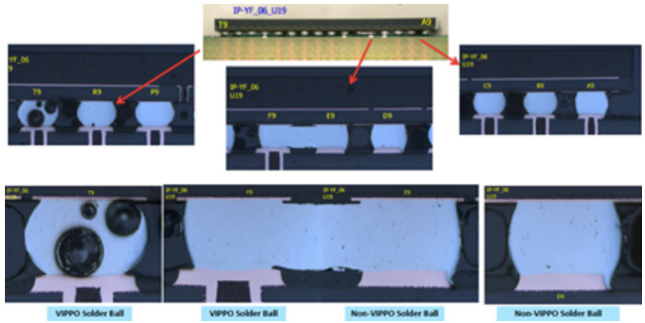

Figure 9: Solder Voiding and Bridging with Solder Joint Encapsulant Material B on DDR4 TV

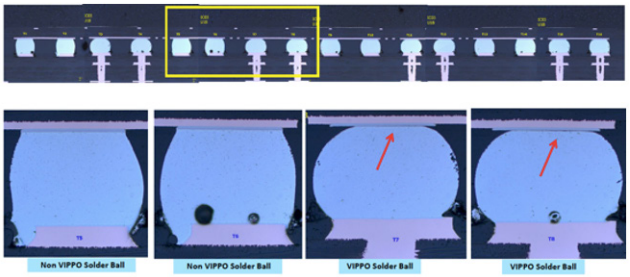

Figure 10: Solder Separation on Fine Pitch TV Control Boards

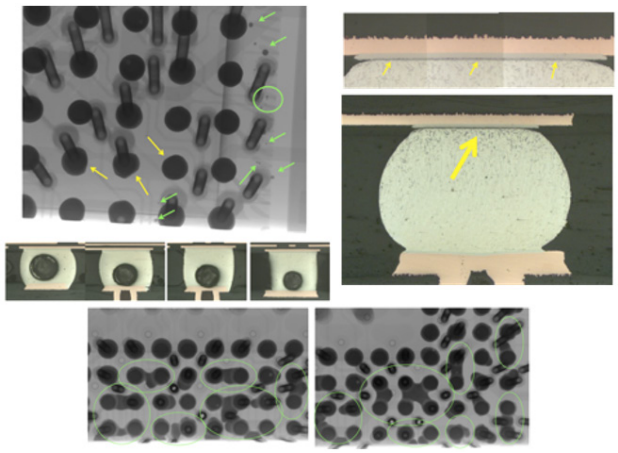

Figure 11: Solder Defects with Solder Joint Encapsulant Material B on Fine Pitch TV Control

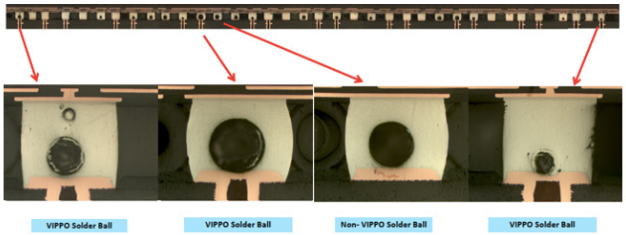

Figure 12: Solder Voiding with Solder Joint Encapsulant Material A on Fine Pitch TV Control

Reliability

The remaining boards for both the DDR4 test vehicle as well as the Fine Pitch test vehicle were submitted for accelerated temperature cycle (ATC) testing per IPC-9701 test conditions of 0°C to 100°C for a minimum of 3500 cycles or 50% failure. The DDR4 test vehicle was assembled with functional parts as daisy-chained components were not available. Therefore, samples of these boards for each of the 3 build legs, control boards with no solder joint encapsulant, boards assembled with solder joint encapsulant material A and boards assembled with solder joint encapsulant material B, were pulled at certain temperature cycle intervals and subjected to physical analysis employing dye and pry or x-section to assess the solder joint integrity. For the Fine Pitch test vehicle, daisy-chained components were available and used for the assembly of these boards. In this case, in-situ resistance monitoring of the daisy-chain nets was utilized to assess the solder joint integrity of each component throughout the ATC testing. The solder joint reliability results for these test vehicles are summarized in Tables 1 and 2.

Table 1: Solder Joint Reliability Comparison for Solder Joint Encapsulant Material A on Fine Pitch TV

Package Type	Control		Solder Paste 1 Solder Joint Encapsulant A		Solder Paste 2 Solder Joint Encapsulant A	
	Beta	Charcteristic Life	Beta	Charcteristic Life	Beta	Charcteristic Life
10mm sq. 0.8mm pitch	*4.7*	*2366*	1.55	754	3.06	1112
15mm sq. 0.8mm pitch	*1.05*	*397*	3.56	445	3.05	649
17mm sq. 1.0mm pitch	0.48	495	3.36	474	1.92	559
19mm sq. 0.8mm pitch	2.76	1077	1.08	648	4.4	625
37mm sq. 0.7mm pitch variable	5.2	1773	*0.7*	*584*	7.41	1537

***Note: Beta < 1 likely due to multiple failure modes (e.g. solder separation defects or assembly defects related to the encapsulant resulting in early failures).**

Table 2: Solder Joint Reliability Comparison for Solder Joint Encapsulant Material B on Fine Pitch TV

Package Type	Control		Solder Paste 1 Solder Joint Encapsulant B		Solder Paste 2 Solder Joint Encapsulant B	
	Beta	Charcteristic Life	Beta	Charcteristic Life	Beta	Charcteristic Life
10mm sq. 0.8mm pitch	*4.7*	*2366*	3.21	1426	2.81	1764
15mm sq. 0.8mm pitch	*1.05*	*397*	4.9	310	0.99	439
17mm sq. 1.0mm pitch	0.48	495	1.7	282	1.13	511
19mm sq. 0.8mm pitch	2.76	1077	7	497	6.01	671
37mm sq. 0.7mm pitch variable	5.2	1773	4.38	1187	3.79	1769

***Note: Beta < 1 likely due to multiple failure modes (e.g. solder separation defects resulting in early failures for control parts).**

The DDR4 test vehicle exhibited similar solder joint reliability among all 3 categories, the control boards with no solder joint encapsulant, boards with solder joint encapsulant material A and boards with solder joint encapsulant material B as well as for both solder pastes. Solder joint crack initiation was identified after 750 cycles with significant solder joint cracking found after 1500 cycles.

The Fine Pitch test vehicle exhibited comparable solder joint reliability between the boards with the solder joint encapsulant materials and the control boards with no solder joint encapsulant material in most cases. Additionally, no specific trend could be identified with the solder paste materials. In a few instances, the characteristic life for a component on the boards with the solder joint encapsulant material(s) was significantly lower than that for the control boards. However, based on initial physical analysis results, it is suspected that assembly defects due to the encapsulant material were likely present for those components which degraded their solder joint reliability. Unfortunately, 5DX inspection or equivalent was not available during the assembly of these test boards and through-scan x-ray data was not retained for reference. Prior to physical analysis with x-sectioning, x-ray inspection was also performed in the FA lab, which identified deformed solder joints and possible solder extrusion through gaps in the coverage of the solder joint encapsulant around the solder joint. Representative images of these possible solder defects are shown in Figures 13 and 14 and representative images of solder joint cracking are presented in Figure 15.

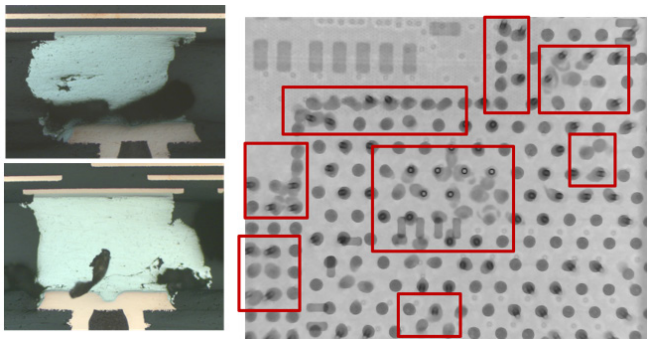

Figure 13: Deformed Solder Joints Found after ATC Testing with Solder Joint Encapsulant Material A

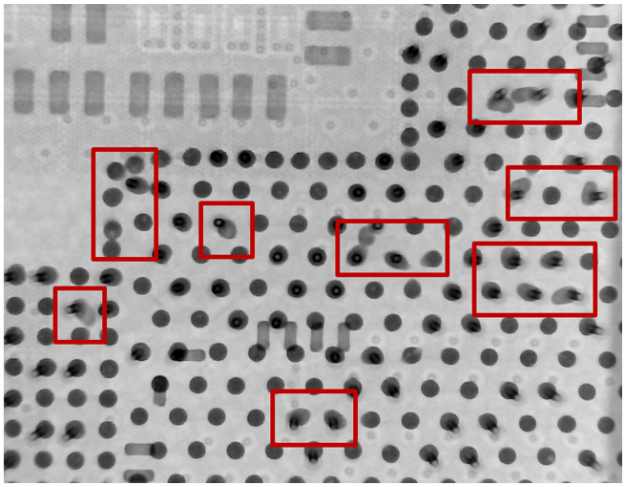

Figure 14: Deformed Solder Joints Found After ATC Testing with Solder Joint Encapsulant Material B

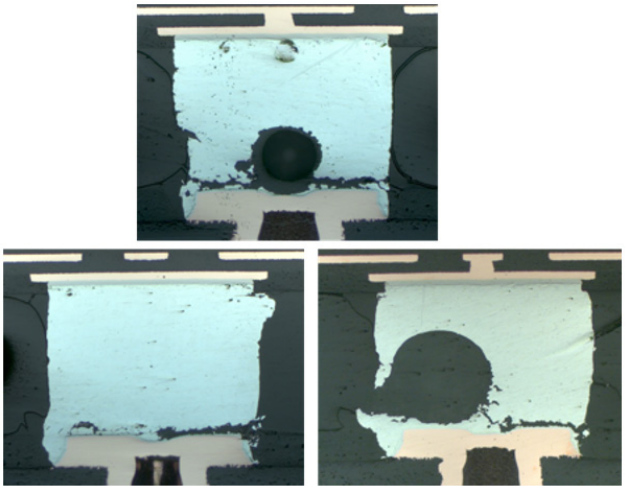

Figure 15: Solder Joint Cracking with Solder Joint Encapsulant Material B After ATC Testing (3500 cycles)

DISCUSSION

This study has shown the solder joint encapsulant material A to be effective in the mitigation of the solder separation defects associated with the use of VIPPO and VIPPO+BD structures within the BGA footprint of a PCB design. This material was also demonstrated to be effective in mitigating HIP defects associated with small, lightweight BGA packages having < 3 mils warpage. These results were consistent across both solder pastes on both test vehicles, as applicable. The solder joint encapsulant material B, however, was found to introduce numerous assembly defects, including solder bridging, deformed solder joints and solder balling, without effectively mitigating either the solder separation defects or the HIP defects. Again, these results were consistent across both solder pastes and both test vehicles. Both solder joint encapsulant materials exhibited significant voiding as compared with the control parts without any solder joint encapsulant. Although the voiding was determined to be within IPC workmanship standards for these test vehicle builds, it was marginal in many instances and may be of concern for a volume production process.

In terms of the influence of these solder joint encapsulant materials on the long-term thermo-mechanical solder joint reliability, initial results from the DDR4 TV suggest that these materials do not have a significant influence on the ATC reliability. For the Fine Pitch TV, which exhibited solder joint defects related to the assembly process with the encapsulant materials, further testing will be needed to characterize the impact of the encapsulant on the solder joint reliability, as there were likely multiple failure modes exhibited in the Weibull distributions. For instance, in the cases showing an appreciable degradation in the characteristic life during ATC testing, the preliminary physical analysis indicates that these early failures are likely due to deformed solder joints resulting from the assembly process rather than conventional solder joint fatigue failures. It is suspected that the volume of the encapsulant material was not consistent across all of the solder joints, possibly due to non-coplanarity of the package, and areas of excessive encapsulant material interfered with proper solder joint formation. The deformed shape of these solder joints does not conform to typical solder joint shapes driven by surface tension. Additional studies should be pursued to further validate this and to investigate further process optimization of the solder joint encapsulant material A to ensure more consistent assembly results.

SUMMARY AND CONCLUSIONS

This work has investigated the assembly performance, defect mitigation effectiveness and influence on long-term solder joint reliability for 2 different solder joint encapsulant materials using 2 different solder pastes. In addition, 2 different test vehicles known to induce the solder separation and HIP defects were utilized in this study, which included control builds without any solder joint encapsulant material and builds with the 2 different solder joint encapsulant materials. In each case, 2 different solder pastes were used in the assembly of each test vehicle.

It was shown that the solder joint encapsulant material A may be a potential solution to mitigate both of the assembly defects

investigated in this study. This material was also demonstrated to be compatible with existing standard production SMT processes. Furthermore, neither solder joint encapsulant material appears to significantly influence the long-term thermo-mechanical solder joint reliability of these packages. However, additional process optimization with the solder joint encapsulant materials would be needed to ensure more uniform solder joint formation for consistent ATC reliability as well as to achieve increased process margins for volume production.

FUTURE WORK

Further development work on the formulation of the solder joint encapsulant material A is being pursued by the material manufacturer to optimize the assembly performance, in terms of the curing behavior and process window. Based on some of the promising results found from this study, future evaluations to characterize the assembly performance of the optimized formulation of this solder joint encapsulant materials may be pursued.

Moreover, since these materials have been shown to provide enhanced adhesion strength for BGA solder joints during SMT reflow, there may be other potential applications for these materials. For instance, the non-wet open defect5 may potentially be mitigated with increased adhesion strength of the solder joint during reflow due to the encapsulant. In addition, as we are seeing increasing usage of bottom-side large body BGA components, particularly with the proliferation of high-speed BGA connectors, the solder surface tension is no longer sufficient to overcome the gravitational force on these components when the board is flipped and put through the top-side reflow process. These solder joint encapsulant materials may prove to be effective in adhering these bottom-side large body BGA components to the board during the top-side reflow process. These potential application areas should be investigated to characterize the effectiveness of these materials in mitigating these other assembly challenges.

ACKNOWLEDGEMENTS

The authors greatly appreciate the support of Paul Ton for consultation on the test vehicle as well as Scott Priore, Sadanand Patil, Kola Akinade, Quyen Chu, Pier Peretta, Roberto Recca and Ashok Singh for the funding and materials support to enable this work.

REFERENCES

1. Teng, S.Y., et al., 'Via-In-Pad Plated Over (VIPPO) Design Considerations for the Mitigation of a Unique Solder Separation Failure Mode', Proceedings of SMTA International, Sept. 2016, pp. 161-167.

2. Chiu, Chun-Chi, el al., 'Fine Pitch BGA Solder Joint Split in SMT process', Proceedings 4th International Microsystems, Packaging, Assembly and Circuits Technology Conference, Oct. 2009.

3. Silk, Julie et al., 'Double Reflow-Induced Brittle Interfacial Failures in Pb-free Ball Grid Array Solder Joints', Proceedings IPC APEX Expo Conference & Exhibition, Feb. 2013, pp.1131-1141.

BIOGRAPHIES

Sue Teng is currently a Sr. Manufacturing Engineer at Google leading printed circuit assembly technology development for next-generation machine learning products to support the Google Cloud infrastructure. Prior to joining Google, she was a technical leader at Cisco Systems, most recently within the Global Manufacturing Operations organization responsible for printed circuit assembly technology development for next-generation semiconductor, interconnect and optics packaging. She has also held various roles within the Technology and Quality organization at Cisco Systems, leading ASIC packaging development and reliability qualification activities as well as interconnect technology reliability characterization. She holds a B.S. and M.S. in mechanical engineering from U. C. Berkeley and has extensive experience in microelectronics packaging, including thermal and thermo-mechanical issues, interconnect reliability and substrate technology.

Cherif Guirguis received his BS degree in Mechatronics engineering from Ecole Polytechnique of Montreal, Canada and an MS degree in Engineering management from Santa Clara University.

Cherif has been working at Cisco for 11 years. He was a senior FA engineer that has been part of Material Science and Failure analysis lab since 2011. His primary focus was on FA support for hardware product development, troubleshooting field returns and line stop/stop ship issues. Cherif is currently working as a Senior Optical Component Engineer handling technical assessment of optical suppliers including next generation technologies and packaging solutions. He has also been assessing reliability risk, developing and executing qualification plans and resolving technical issues. Cherif has co-authored over 15 publications and articles and is a member of SMTA.

Gnyaneshwar Ramakrishna, serves as a Technical Leader overseeing component qualification and reliability at Cisco Systems. His experience ranges from high speed packaging, photonics packaging, connectors, power supplies focusing on product delivery over the past 18 years. In addition, he serves as chair for Photonics technical committee in IEEE-EPS. He holds an MBA from Santa Clara University, Master's in Mechanical engineering from Georgia Tech and Bachelors from IIT-Madras.

Hien Ly has worked in the manufacturing engineering sector for over 28 years. He is currently the engineering manager at Jabil, helping to drive new technology innovations. His competencies are supported by a Bachelor of Science Degree in Electrical Engineering, 8 years of industrial engineering experience in Original Equipment Manufacturer (OEM) production, and 20+ years of Surface Mount Technology (SMT) manufacturing experience. His other capabilities include adaptation to new technologies and broad knowledge of mechanical and electronic devices.

He is a member of the Institute of Electrical and Electronics Engineers (IEEE) and was a participant in Technical Committee of IEEE International Reliability Physics Symposium (IRPS). He has also published and co-authored articles in SMT Magazine and presented at SMTA conferences.

In his spare time, he likes to listen to music and play music instruments. He also likes to work on home improvement projects, automotive maintenance, and home electronic equipment.

QUALITATIVE MODEL DESCRIBING HOT TEAR ABOVE VIPPO AND NUMEROUS OTHER DESIGN ELEMENTS

Günter Gera, Udo Welzel, Yin Jizhe and Harald Feufel
Robert-Bosch GmbH

ABSTRACT

Over the last couples of years there have been numerous reports of a unique soldering failure resulting in a separation of BGA solder joints from the intermetallic compound at the interposer during reflow. In most cases, the failures were correlated with the use of Via-In-Pad-Plated-Over-Technology. Since the separation could be proven to occur during the phase transition from solid to liquid [1] the term Hot Tear was used. Even though this term is traditionally only used for tears during solidification its scope was extended to tears during any phase transition. Since the Hot Tear results in a very thin separation it is usually not inspectable, neither by means of X-Ray inspection nor by electrical testing, but results in very early field failures.

In this paper, the general mechanism for the formation of Hot Tears will be discussed and applied to numerous other design elements that can be found on Printed Circuit Board Assemblies. We will show that due to several industry trends e.g. VIPPO, heavy copper PCBs, buried vias, non-eutectic alloys, thinner components, thicker boards, via in pad, etc. the probability of Hot Tears is steadily increasing.

Key words: VIPPO, Hot Tear, Solder, Separation, Reflow Soldering, BGA, Fillet Lifting, ePad

INTRODUCTION

Today's electronic devices mainly consist of Printed Circuit Board Assemblies (PCBAs), where solder joints are the most common way to connect the electronic components with the Printed Circuit Board (PCB). In order to avoid early field failures due to shorts and open circuits the PCBAs are typically inspected for misplaced components, insufficient solder, wetting failures, etc. Failure modes, which cannot be inspected after production, have to be thoroughly understood and avoided by design. Since Hot Tear results in a separation between solder and IMC, which is so thin that it can neither be inspected by optical inspection (AOI), X-ray inspection (AXI) nor electrical testing (ICT) it has to be avoided by design. (See Fig 1).

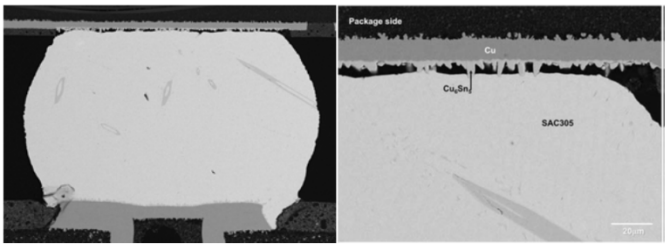

Figure 1: Very thin separation between Solder and IMC due to Hot Tear Defect (taken from [2] with permission)

Cohesive Hot Tear in Bulk

The most common form of Hot Tear is the shrinkage crack – a cohesive tearing in the bulk of the material during solidification. It is mainly known as a casting defect, but is also observable in solder joints. According to IPC-A-610 "there is no defect associated with this anomaly, provided the connection meets all other acceptance criteria." [3] Even though shrinkage cracks are most common in solder joint manufactured via Through Hole Technology (THT), they can also be observed in almost any other design situation.

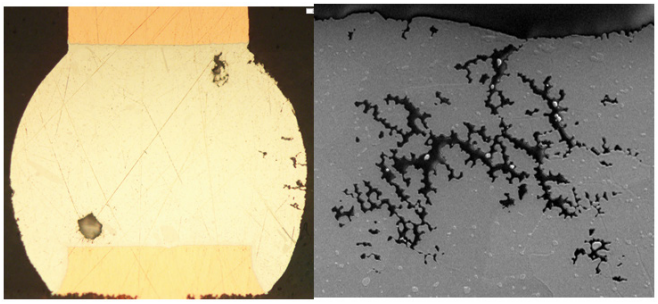

Figure 2: Hot Tear in the bulk solder of a BGA solder joint and in an exposed Pad solder joint.

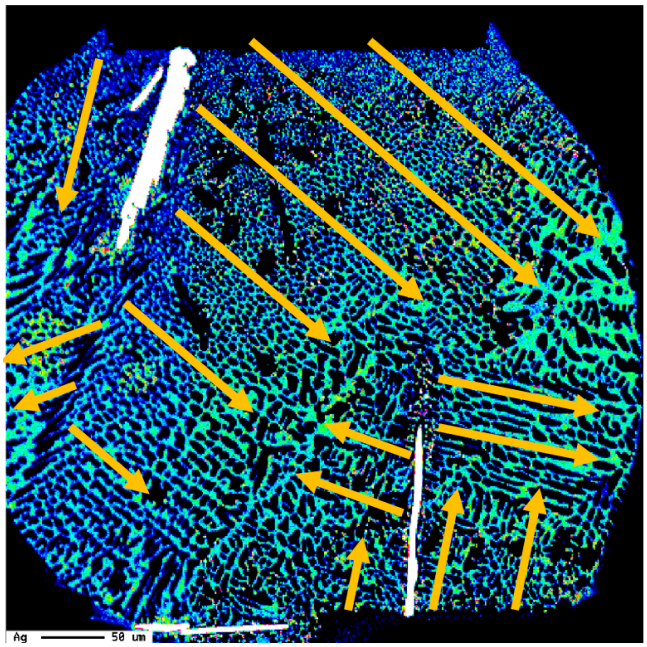

Figure 3: Electron Probe Micro Analysis (EPMA) of a SnAg3.5Cu0.7 - BGA ball. Coloring represents Ag content. Yellow arrows represent derived directions of solidification.

Looking at the microstructure of a solder joint, it is possible to understand why Hot Tears form in bulk solder. The direction of solidification is always along the lines of the laminar Ag_3Sn structures from fine to coarse. Since the heat leaves the BGA ball mainly through the copper pads it can be observed that the solder starts to solidify at those pads (see Fig.3). The last parts, which solidify are at the edge of the ball. Since there is no liquid solder left to feed the solidification shrinkage a Hot Tear is likely to occur (see Fig. 2).

Adhesive Hot Tear at Interfaces

Though the cohesive Hot Tear of the bulk solder is most common it usually does not have any influence on the reliability of the solder joints, because crack paths due to environmental stress are typically close to one of the terminations of the solder joint. The most commonly known Hot Tear at an interface of the Solder Joint is the Fillet Lifting of a THT solder joint (see Fig.4). According to IPC-A-610 "There is no defect associated with this anomaly." provided the connection meets all other acceptance criteria. [2]

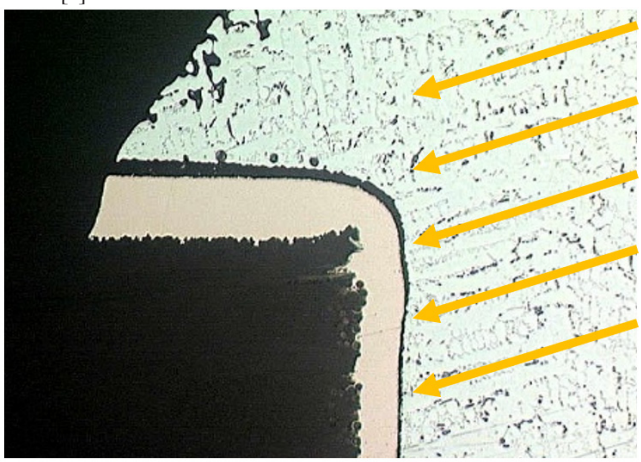

Figure 4: Fillet Lifting observed at a SnAgCu THT solder joint. Yellow arrows represent derived directions of solidification.

Since the solidification is directional, the last point of solidification is at the termination of the PCB. If no liquid solder is available to feed the gaps a Hot Tear can occur.

MODEL FOR HOT TEAR AT INTERFACES

Theoretical Model

As already observed for shrinkage cracks and fillet liftings Hot Tears occur during the phase transition, while the solder is "Hot". As the word "Tear" implies, some kind of tensile stress has to be applied during this phase transition. Looking at the material properties of solid and liquid solder it is possible to understand the mechanism.

Due to the high Young's modulus E the deformation ε of the solid solder is always well below the elongation at fracture ε_f. Hot Tear is therefore not possible (see Fig. 5).

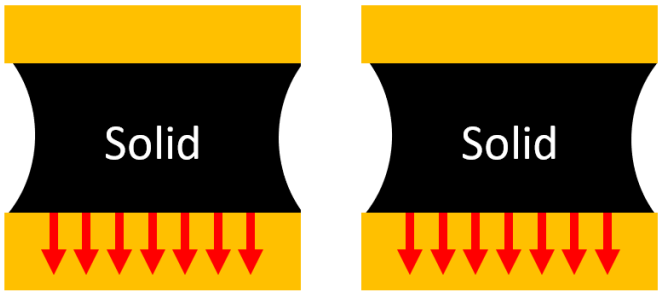

Figure 5: Tensile stress on the solid solder joint does not result in a significant deformation

The stress necessary to deform the liquid solder can be described using the Young-Laplace equation [5]

$$\sigma = \gamma\left(\frac{1}{R_1}+\frac{1}{R_2}+u\right) \approx \gamma\frac{2\,Cos(\theta)}{h(1+\varepsilon)},$$

where γ is the surface tension of the solder, u is the circumference of the solder joint and R_1 and R_2 are the local radii of curvature of the solder joint surface. Using the wetting angle θ for a small stand-off height h it is possible to describe this stress as a function of the elongation ε. Even though this stress is much lower than for the solid solder it is usually not possible to achieve a Hot Tear, because of the very large elongation at fracture ε_f (see Fig.6).

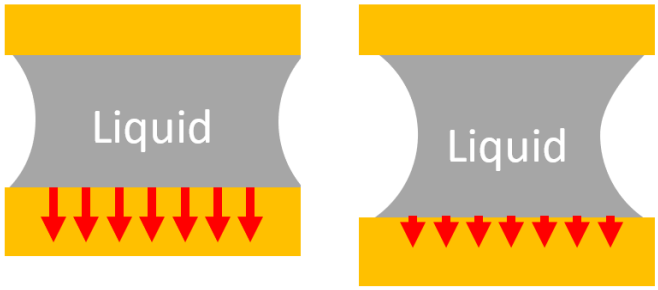

Figure 6: Tensile stress on the liquid solder joint results in a significant deformation, but is usually not able to break the liquid bridge.

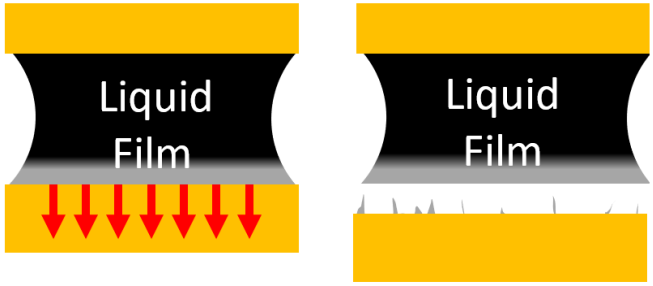

Figure 7: Tensile stress on the liquid film results in a significant deformation. The film will break from the adjacent termination.

In case the solder joint solidifies directionally, the thickness of the liquid film becomes gradually thinner during this process. This will slightly increase the Young-Laplace pressure necessary to deform the surface, but leaving it still orders of magnitude below that of the solid solder. If the liquid film is very thin right before the complete solidification, the amount of liquid solder is insufficient to feed the gaps resulting in a very low elongation at fracture ε_f (see Fig.7). All three situations can be visualized as graphs in a common stress-strain diagram (see Fig.8).

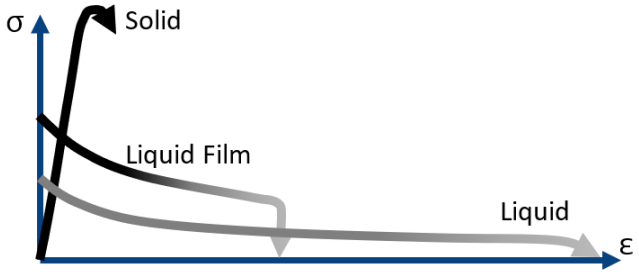

Figure 8: Stress-strain diagram for solid solder, liquid solder and a liquid solder film.

DIRECTIONAL PHASE TRANSITIONS

Liquid Films

To achieve the thin liquid films, which are mandatory for the occurrence of adhesive Hot Tear, either a directional solidification or a directional melting is required. If the hot tear is formed due to directional melting, it occurs in the area where the melting first occurs (typically at the interface between the solder and intermetallic.) If the hot tear is formed due to directional solidification, it occurs in the area that solidifies last (mostly a free surface of the solder joint, but in some cases also at one of the interfaces between the solder and intermetallic.) Both mechanisms are driven by a temperature gradient ∇T that can in one dimension be transformed to $\nabla T \xrightarrow{1d} \frac{\Delta T}{d}$, where ΔT is the temperature difference and d is the distance between the solder joint terminations. A sufficient temperature gradient for the directional phase transition will be achieved, if either the temperature difference ΔT is very big or the distance d is very small. Examples will be discussed in the following sections.

THT solder joints

Large differences in temperature ΔT can typically be observed if heat is inserted at one specific point. The most prominent example is THT soldering. While the electronic components at the top side of the PCB stay relatively cool, heat is inserted through the wave of liquid solder at the bottom of the PCB. Additionally, the heat capacity of the PCB is larger than the heat capacity of the pin. This results in a solidification path from top to bottom and from inside to outside. Inner layers can act as local heat capacitities, changing the path of solidification (see Fig.9).

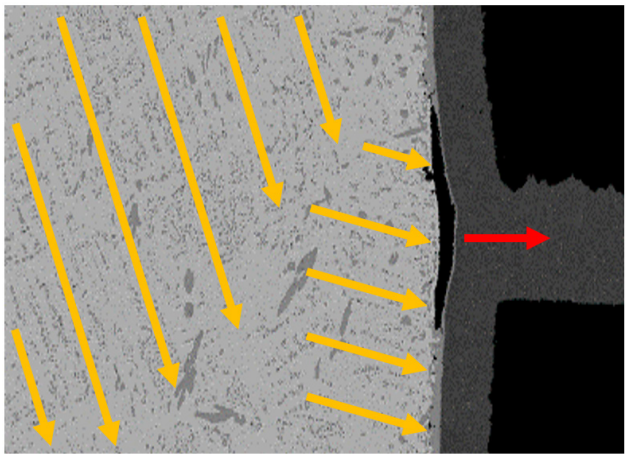

Figure 9: Directional solidification of a THT solder joint (represented by yellow arrows). Tensile stress due to PCB shrink (represented by red arrows).

SMT solder joints after THT soldering

A rather ununsual exaple for a directional phase transition is the melting of an SMT solder joint due to heat from the THT soldering process. The heat is conducted through the PCB and, if a sufficient temperature is reached, the solder joint will melt from the bottom. The thin liquid film in combination with the tensile stress due to component warpage results in the formation of a Hot Tear failure.

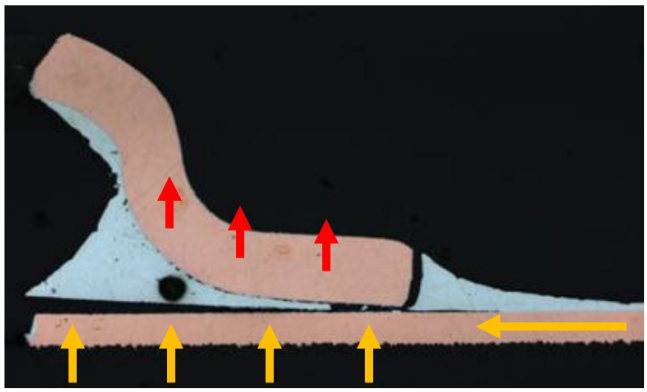

Figure 10: Directional melding of a SMT solder joint due to heat from the THT soldering (represented by yellow arrows). Tensile stress due to component warpage (represented by red arrows).

SMT solder joints

Typically, during the SMT process the heat is transferred via convection of hot gas (e.g. air or nitrogen). In some cases due to geometrical restrictions, it is not possible to guarantee sufficient flow of hot gas between the PCB and the component. Especially, in case of area array components and exposed pads, the heat is mainly transferred by means of conduction through the PCB and the electronic component. Since the heat is inserted through the termination of the solder joint that is also where the melting of the solder joint starts. If the surface area of the termination is very small, it is very likely that a complete thin liquid film forms (see Fig.11).

In case the solder joint solidifies directionally, the thickness of the liquid film becomes gradually thinner during this process. This will slightly increase the Young-Laplace pressure necessary to deform the surface, but leaving it still orders of magnitude below that of the solid solder. If the liquid film is very thin right before the complete solidification, the amount of liquid solder is insufficient to feed the gaps resulting in a very low elongation at fracture ε_f (see Fig.7). All three situations can be visualized as graphs in a common stress-strain diagram (see Fig.8).

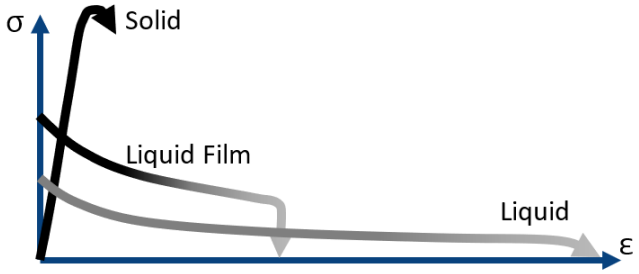

Figure 8: Stress-strain diagram for solid solder, liquid solder and a liquid solder film.

DIRECTIONAL PHASE TRANSITIONS

Liquid Films

To achieve the thin liquid films, which are mandatory for the occurrence of adhesive Hot Tear, either a directional solidification or a directional melting is required. If the hot tear is formed due to directional melting, it occurs in the area where the melting first occurs (typically at the interface between the solder and intermetallic.) If the hot tear is formed due to directional solidification, it occurs in the area that solidifies last (mostly a free surface of the solder joint, but in some cases also at one of the interfaces between the solder and intermetallic.) Both mechanisms are driven by a temperature gradient ∇T that can in one dimension be transformed to $\nabla T \xrightarrow{1d} \frac{\Delta T}{d}$, where ΔT is the temperature difference and d is the distance between the solder joint terminations. A sufficient temperature gradient for the directional phase transition will be achieved, if either the temperature difference ΔT is very big or the distance d is very small. Examples will be discussed in the following sections.

THT solder joints

Large differences in temperature ΔT can typically be observed if heat is inserted at one specific point. The most prominent example is THT soldering. While the electronic components at the top side of the PCB stay relatively cool, heat is inserted through the wave of liquid solder at the bottom of the PCB. Additionally, the heat capacity of the PCB is larger than the heat capacity of the pin. This results in a solidification path from top to bottom and from inside to outside. Inner layers can act as local heat capacitities, changing the path of solidification (see Fig.9).

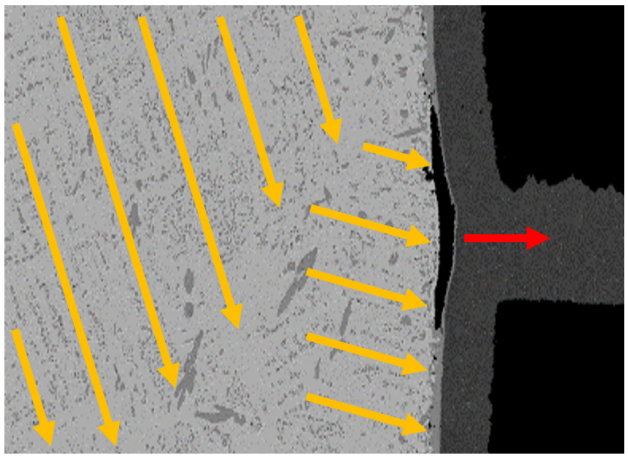

Figure 9: Directional solidification of a THT solder joint (represented by yellow arrows). Tensile stress due to PCB shrink (represented by red arrows).

SMT solder joints after THT soldering

A rather ununsual exaple for a directional phase transition is the melting of an SMT solder joint due to heat from the THT soldering process. The heat is conducted through the PCB and, if a sufficient temperature is reached, the solder joint will melt from the bottom. The thin liquid film in combination with the tensile stress due to component warpage results in the formation of a Hot Tear failure.

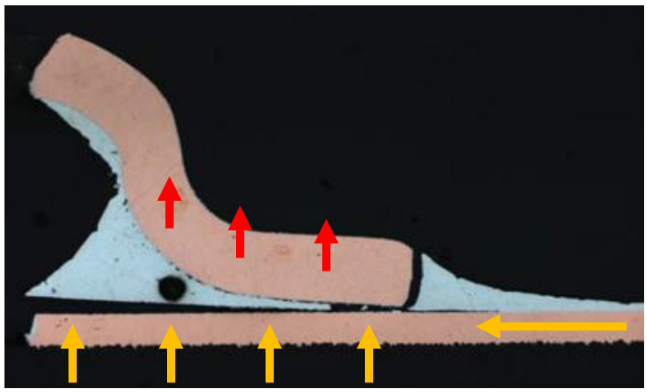

Figure 10: Directional melding of a SMT solder joint due to heat from the THT soldering (represented by yellow arrows). Tensile stress due to component warpage (represented by red arrows).

SMT solder joints

Typically, during the SMT process the heat is transferred via convection of hot gas (e.g. air or nitrogen). In some cases due to geometrical restrictions, it is not possible to guarantee sufficient flow of hot gas between the PCB and the component. Especially, in case of area array components and exposed pads, the heat is mainly transferred by means of conduction through the PCB and the electronic component. Since the heat is inserted through the termination of the solder joint that is also where the melting of the solder joint starts. If the surface area of the termination is very small, it is very likely that a complete thin liquid film forms (see Fig.11).

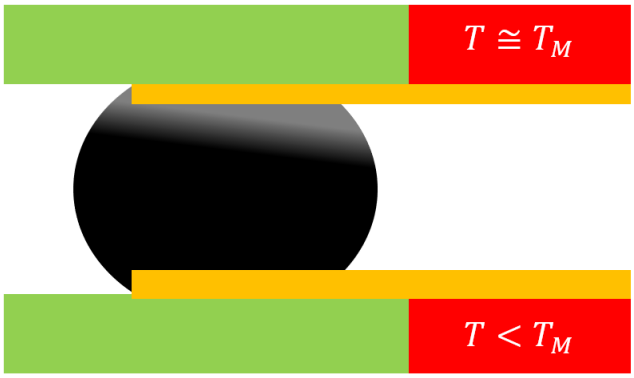

Figure 11: Schematic picture of the directional melting of a BGA solder joint.

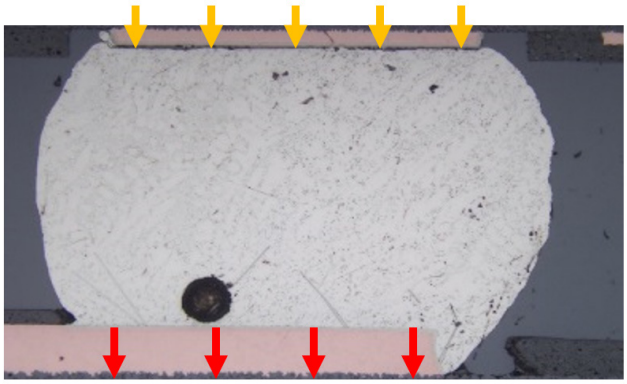

Figure 12: BGA ball with Hot Tear. Yellow arrows represent directional melting. Red arrows represent tensile stress.

Small standoff

Even if the temperature difference ΔT is rather small, the small standoff d in exposed pad solder joints can still create a sufficiently large temperature gradient VT for directional solidification. Since this process is highly sensitive to small changes in temperature, heat capacity and cooling, it is possible to observe both directions of solidification (see Fig. 13 and 14).

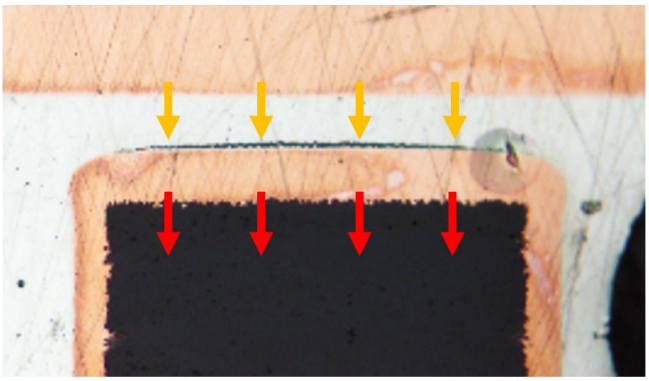

Figure 13: Exposed Pad solder joint with Hot Tear. Yellow arrows represent solidification from top to bottom. Red arrows represent tensile stress.

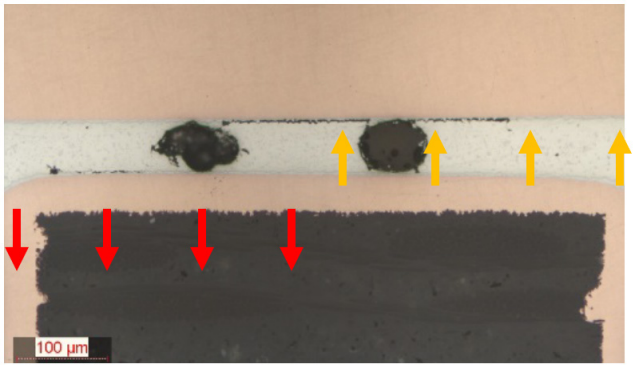

Figure 14: Exposed Pad solder joint with Hot Tear. Yellow arrows represent solidification from bottom to top. Red arrows represent tensile stress.

LOAD

Tensile Stress

Whether a liquid film actually results in a Hot Tear strongly depends on the amount of tensile stress applied. If the tensile stress is insufficient to overcome the capillary pressure, no Hot Tear forms (see Fig. 15a). Intermediate loads will result in a deformation of the liquid film and in tiny depletion voids near the solder-intermetallic interface, but not in a full-grown Hot Tear (see Fig. 15b). Only if the load is sufficient to completely severe the thin liquid film, a Hot Tear will form in a larger area (see Fig. 15c).

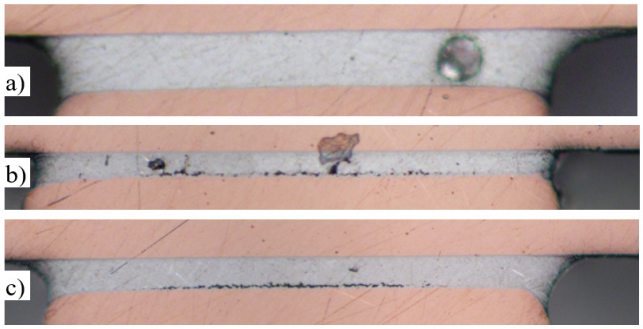

Figure 15: a) Solder joint without Hot Tear b) Solder joint with localized Hot Tear spots c) Solder joint with large area of Hot Tear .

The load can also be visualized as graphs in the stress-strain diagram. The cross section with the x-axis represents the elongation in a stress free system. The slope of the load graph represents the total elastic modulus of the system surrounding the solder joint. If there load graph is below the graph of the liquid film this load is too low to affect the liquid film (see Fig. 16a). If there load graph is above the graph of the liquid film this load is too high for the liquid film – a complete Hot Tear occurs (see Fig. 16c). If there is an intersection between the load graph and the graph of the thin liquid film this means that some part of the film still holds, but the film is elongated resulting in depletion voids (see Fig. 16b).

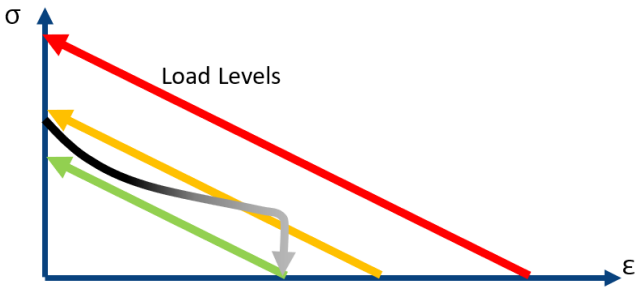

Figure 16: Stress-strain diagram for a liquid solder film and three different load levels. a) The green graph represents an uncritical load. b) The yellow graph represents a load resulting in partial Hot Tear. c) The red graph represents a load resulting in a full Hot Tear.

PCB induced Stress during cooling

Tensile stress on solder joints is almost unavoidable. This stress can originate from the solidification shrinkage of the solder alloy itself, or from the warpage of electronic components on the board. Next to those two well-known sources, there is also the possibility that tensile stress is induced by the local deformation of the PCB. This can be the case if there are big variations of copper content below a solder joint. While the coefficient of thermal expansion (CTE) of copper is 16 ppm/K, the CTE perpendicular to the surface of the PCB above the glass transition temperature T_G can be up to 200ppm/K. During the solidification of the solder joint this results in a bigger shrinkage of the parts above the base material, compared to the areas above the copper. If the solder solidifies directionally, a Hot Tear can occur (see Fig. 17).

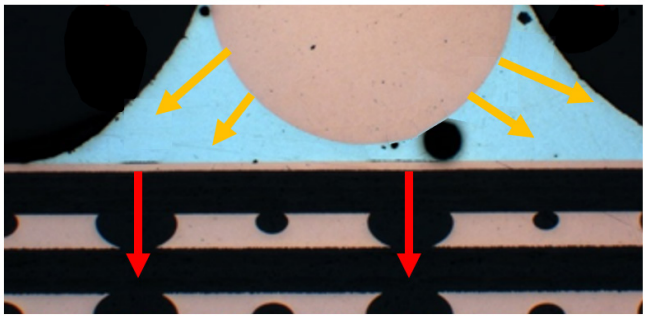

Figure 17: Hot Tear above areas with lower copper content in the PCB inner layers. Yellow arrows represent directional solidification. Red arrows represent tensile stress.

Luckily, this effect usually does not occur with eutectic and nearly eutectic solder alloys such as SAC or SnPb. The reason is the temperature range in which the thin liquid film exists. For nearly eutectic alloys, the temperature difference between solidus temperature T_S and liquidus temperature T_L is very small. Even with the huge CTE mismatch between PCB base material and copper, the displacement ε that can be reached is very small. The load is not sufficient to create a Hot Tear.

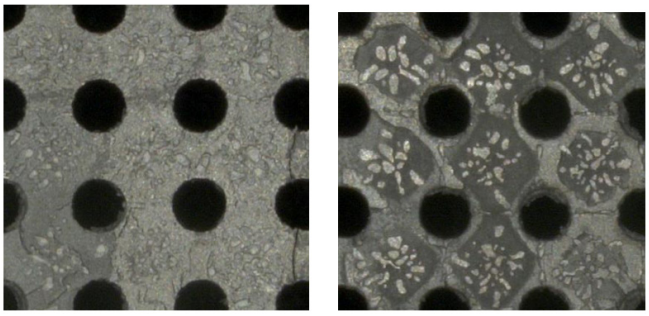

Figure 18: Exposed Pad solder joints with via in pad design that had the component pulled from the PCB. Black areas are Plated Through holes. Light gray areas are soldered areas. Dark gray areas are Hot Tear. The left solder joint was soldered with SAC305 and the right with Innolot.

Advanced alloys (e.g. Innolot, SnCuIn, etc.) are usually not a eutectic composition. Typically the difference between solidus and liquidus can be 10K and more. During the phase transition, the first dendritic structures starts to solidify after passing the liquidus. Those phases hinder a further sinking in of the electronic component. Tensile stress can build up until the solidus is reached (see Fig. 19). Due to the larger temperature difference, the tensile stress can be more than 10 times higher for non-eutectic alloys than for nearly eutectic alloys.

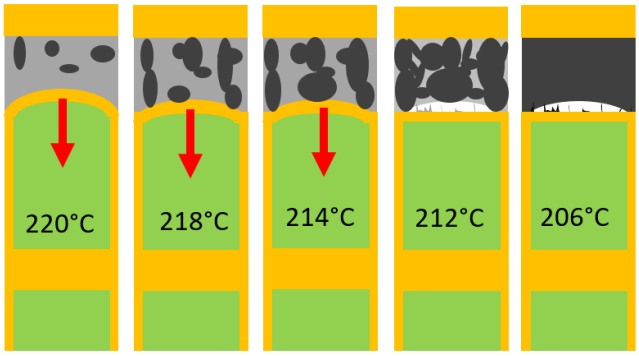

Figure 19: During cooling, the tensile stress can build up between liquidus and solidus. For non-eutectic alloys, the stress is much higher due to the larger melting range.

PCB induced Stress during cooling

Analog to the tensile stress during cooling, tensile stress can also be invoked during heating. Whereas, the tensile stress and thus the Hot Tear always occurs above regions with less copper content in case of cooling. In case of heating it is the other way around. Areas with low copper content expand much more during the reflow process (see Fig. 20).

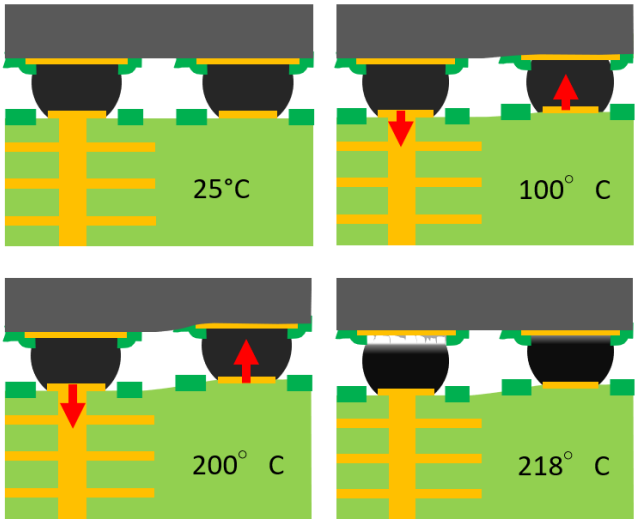

Figure 20: During the heating, the tensile stress can build up between room temperature and Solidus. After passing Solidus, a Hot Tear will form if a thin liquid film is present.

Since in case of heating the solder joints are solid over the complete range from room temperature until solidus the tensile stress can build up over this complete range. Accordingly, the stresses due to this expansion of the PCB are much higher than during cooling. Even deformation of the interposer has been observed [4].

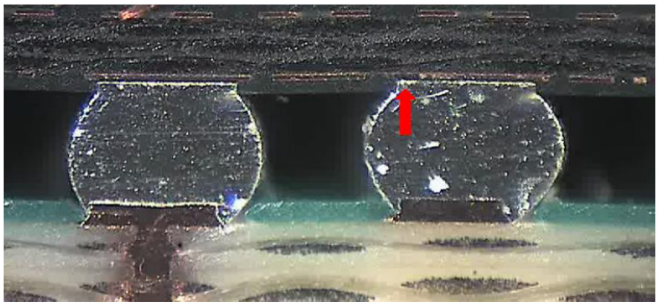

Figure 21: Cross Section of BGA with mixed VIPPO/non-VIPPO technology heated up just below Solidus. The red arrow marks the visible deformation of the BGA Interposer due to the stress induced by the PCB expansion (taken from [2] with permission).

It is often observed that Hot Tear failures at BGA balls only occur during the second reflow process [1]. This can be understood, if we keep in mind that only during the melting of the second reflow we have both, a directional melting and a tensile stress. During the melting of the first reflow, the solder paste is not able to transfer the tensile stress and directional solidification is very unlikely due to the large height of the BGA solder joint.

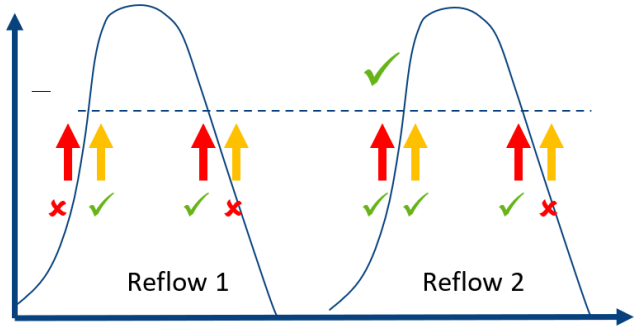

Figure 22: Schematic of two reflow profiles.

CONCLUSION

The understanding of the failure mode Hot Tear has been extended from cohesive tearing during the solidification of liquid material to all possible forms of tearing - cohesive and adhesive – during the phase transition both from solid to liquid and from liquid to solid. It could be shown that for the Hot Tears a thin liquid film needs to be present. Adhesive Hot Tears occur if the liquid film forms near one of the interfaces by means of directional melting or solidification. The temperature difference ΔT and the thickness of the solder joint d could be identified as the main influencing factors on the directional phase transition. The tensile stress necessary for the formation of Hot Tears can originate either from the component, the solder material itself or from the PCB. With respect to PCB induced stress, it could be shown that local variations of the copper content have a strong impact on the thermal expansion perpendicular to the PCB surface. With this qualitative model, it is possible to completely understand the formation of Hot Tears of BGA balls on mixed VIPPO/non-VIPPO designs during the second reflow. In the future this qualitative model has to be verified and quantified by collecting data using experimental or simulative methodologies.

REFERENCES

[1] Steven Perng, Weidong Xie et al., "Innovative BGA defect detection methode for transient discontinuity", in SMTA International Conference, 2015

[2] Steven Perng, Weidong Xie et al., "Transient Solder Separation of BGA Solder joint During Second Reflow Cycle", Circuit Insight, 2016

[3] IPC-A-610 G, "Acceptability of Electronic Assemblies," IPC, March 2017.

[4] S.Y. Teng, P. Peretta and P. Ton, Cisco Systems Inc.; and V. Kome-ong and W. Kamanee, Celestica Thailand, "Via-in-Pad Plated over Design Considerations to Mitigate Solder Separation Failure" smt.iconnect007, 2017

[5] P. S. Laplace, Traité de Mécanique Céleste, Paris: Gauthier-Villars, 1839.

Welcome New SMTA Members!

GENARO A ALCALA SOTO
ITW Contamination Control Electronics
Ciudad Juarez, Mexico

Tom Anderson
Keysight Technologies
Santa Rosa, CA

Cheng Hui Simon Ang
DSO National Laboratories
Singapore, Singapore

Bob Asanuma
Keysight Technologies
Santa Rosa, CA

Salvador Ávila
Universidad Tecnológica de Juárez
Cd. Juárez, Mexico

James Ayars
JJ Technologies
Wareham, MA

Steven Baker
Techni-Tool
Worcester, PA

Robert Barrett
Saki
Surprise, AZ

Richard Bellemare
MacDermid Alpha
Waterbury, CT

karnpal Bhathal
Fabrinet
San Jose, CA

Randy Bremner
Northrop Grumman
Salt Lake City, UT

Matt Brown
Wavetronix
Springville, UT

Antonio Cabrera
ACTnano
Naucalpan, Mexico State, Mexico

Scott Cain
KYZEN Corporation
Napa, CA

Jan Cameron
Patterson and Sheridan LLP
Houston, TX

ZIMAO JOHN CAO
Bisonland Industries Corp
Auburn, WA

Robert Carlsson
CPAC Systems AB
Molndal, Sweden

Vincent Carrigan
AOI SYSTEMS
Davenport, FL

Mac Carson
GHSP
Grand Haven, MI

Cassie Cauley
KYZEN Corporation
Nashville, TN

Alvin Ch-Loo
Keysight Technologies
Santa Rosa, CA, Singapore

Jason Chan
KYZEN Taiwan
Taoyuan District, Taoyuan, Taiwan

Forrest W. Christian
Innovation Machine, Ltd
Helena, MT

Mike Cilia
Juniper Networks
Sunnyvale, CA

Joseph C Cionni
L3HARRIS
Cincinnati, OH

Reggie Clark
Curtiss-Wright
Salt Lake City, UT

Kevin Connors
University of Minnesota
Minneapolis, MN

Traian Cucu
MacDermid Alpha Electronics Solutions
Budd Lake, NJ

Mabel De-Cunha
Keysight Technologies
Bayan Lepas, Malaysia

Angel Deluna
Circuit Technology, Inc.
Holly Springs, NC

Cassandra Diaz
Kurt Whitlock Associates
St. Cloud, FL

Brandon Brownell Dickerson
nScrypt
Orlando, FL

Do Dinh
Ducommun
Tulsa, OK

Mike Duddy
WORLD Electronics
Reading, PA

Aisha Elaine Edwards
Apollo America
Pontiac, MI

Dirk C. Ellis
KYZEN Corporation
Nashville, TN

Emuobosan Enakerakpo
SUNY Binghamton
Johnson, NY

Dan Evans
Saelig Company Inc.
Fairport, NY

William Robert Everett II
Moog Space and Defense
East Aurora, NY

Glenn Fager
Smiths Medical
Oakdale, MN

Abdullah Fahim
Auburn University
Auburn, AL

Shelley Fitzgerald
Raytheon
Dracut, MA

Keith Furr
MacDermid Alpha Electronics Solutions
Hebron, KY

Sandeep Gaan
Intel Corporation
Chandler, AZ

Norbert Galster
Atotech Deutschland GmbH
Basel, Mattenstrasse Postfach, Switzerland

Kishan Ghadiya
AalokTronix Inc.
Seattle, WA

Bob Gilbert
FCT Assembly
ALBA, TX

Josh Gong
Keysight Technologies
Santa Rosa, CA

Rodolfo González
Repstronics
ZAPOPAN, JA, Mexico

Scott Gregg
BAE Systems
Dallas, TX

Rich Gregorski
Epec Engineered Technologies
New Bedford, MA

Tait Gripp
Ducommun
Tulsa, OK

Brett Hall
Glentek
El Segundo, CA

Joshua Hall
KMC Controls
New Paris, IN

Joel Humes
Keysight Technologies
Santa Rosa, CA

Ioannis Ipliktsiadis
LandisGyr
Corinth, Greece

Sebastian Iturregui-Shelton
Rochester Institute of Technology
Brooklyn, NY

Javier Jamaica
SCHUNK Mexico
Querétaro, Mexico

Prabhat Janamanchi
University of Maryland
College Park, MD

Se Young Jang
Seoungnam, , Republic of Korea

Qian Jiang
University of Maryland, College Park
College Park, MD

Ricardo Jimenez
Creation Technologies Inc.
Wheeling, IL

Haley Jones
KYZEN Corporation
Nashville, TN

Mehzabeen Kabir
University of Texas at Arlington
Arlington, TX

Manohar Karande
Juniper Networks
Bangalore-Karnataka, India

James David Keeland
Benchmark Electronics, MN Division
Angleton, TX

Munychort Korn
Jabil Circuit, Inc.
San Jose, CA

Boey Kuek
KYZEN Sdn. Bhd.
Bayan Lepas, Penang, Malaysia

Dinesh Kumar
SL Lumax
Chennai, Tamil Nadu, India

Janani Kumar
Keysight Technologies
Santa Rosa, CA

Andrey Lee
Keysight Technologies
Penang, Malaysia

Scott Lewin
MacDermid Alpha Electronics Solutions
Carmel, IN

David Lober
KYZEN Corporation
Nashville, TN

BHUSHAN LOHANI
University of Texas at El Paso
El Paso, TX

Cedric Lopez
Actia Automotive
COLOMIERS, France

Sophy Luo
GOLDLAND ELECTRONIC TECHNOLOGY
shenzhen, , China

Rachit Malik
Intel Corporation
Hillsboro, OR

Jarred Mandel
REStronics
Mount Kisco, NY

Mark Mankoura
AT&A
DDO, QC, Canada

Roman Maravilla
Murata Electronics
Carrollton, TX

Agustin Marcelino Córdova
MAHA SOLUCIONES INTEGRALES PARA LA INDUSTRIA SAS D
Reynosa, Mexico

Tim Martin
Sencon Inc
Bedford Park, IL

Marcos Iram Martínez Gómez
Valeo
San Luis Potosi, San Luis Potosi, Mexico

Vincent McGee
Epec
New Bedford, MA

Andy Meyer
Honeywell FM&T
Kansas City, MO

Aaron Morgan
GHSP
Grand Haven, MI

Chris Mueller
Global Traffic Technologies
St. Paul, MN

Balan Murthy
Western Digital
Penang, Malaysia

Samy Nashabe
Computrol
Thornton, CO

Danny Ngan
KYZEN Sdn. Bhd.
Bayan Lepas, Penang, Malaysia

Danah Omary
University of North Texas
Denton, TX

Wei-Han Ong
Keysight Technologies
Bayan Lepas, Malaysia

Manuel Alberto Osuna
Macdermid Alpha
general escobedo, , Mexico

Rafael Padilla Jr.
MacDermid Alpha Electronics Solutions
San Leandro, CA

Kyler Page
Ducommun
Tulsa, OK

Honey Sara Paulose
Sheridan College
Brampton, ON, Canada

Yong Pei
University of Maryland
College Park, MD

Mario Perez
Schneider Electric
Rio Bravo, Tamaulipas, Mexico

David Phillips
Creation Technologies
Markham, ON, Canada

Dan Prezioso
Juniper Networks
Westford, MA

Elanggovan Ramasamy
Juniper Networks
Kuala Lumpur, Malaysia

Rob Reeves
KYZEN Corporation
Nashville, TN

Christopher Riso
UMD college park
Washington, DC

Lisa Rizzo
HZO
Burlington, NC

RAGHABENDRA ROUT
Binghamton University-SUNY
Fremont, CA

Lily Sanarajoo
KYZEN
Bayan Lepas, Penang, Malaysia

Andrew Santellan
GHSP
Grand Haven, MI

Jody Saultz
Kyzen
St Cloud, FL

Adam Shoukry
Vicor Corp
Northborough, MA

Saurabh Shrivastava
MacDermid Alpha Electronics Solutions
Bangalore, Karnataka, India

Hardip Singh
KYZEN Sdn. Bhd.
Bayan Lepas, Penang, Malaysia

Richard Stephenson
EMD Performance Materials - Ormet Circuits
San Diego, CA

Lisa Stickley
Weller Tools
Lexington, SC

James Stockhausen
Chemark Consulting Group
Ballwin, MO

Nick Stolper
Panasonic
Rolling Meadows, IL

Steve Stonebraker
Omega Electronics Reps
MALVERN, OH

Sriranjani Sundareshan
Thales India Pvt. Ltd.
Bengaluru-560 025. INDIA, , India

IYEN SUNG
Askey
Suzhou, Jiangsu Province, China

Charles Terrell Swanson CSMTPE
Rockwell Automation
Mayfield Heights, OH

Will Sweet
KYZEN
Nashville, TN

Alexandra Tagscherer
SMT North America, Inc.
Richmond, VA

Yonas Tamyalew
University of Maryland
College Park, MD

James Teoh
KYZEN Sdn. Bhd.
Bayan Lepas, Penang, Malaysia

Jenn Teoh
KYZEN Sdn. Bhd.
Bayan Lepas, Penang, Malaysia

Chad Tipton
CACI
Aberdeen, MD

Erik Michael Trett
Von Roll USA
Indialantic, FL

Ta Tuan
Hai Phong University
Hai Phong, , Vietnam

Travis Vanover
GHSP
Grand Haven, MI

Alex Volovich
WET
Sun Valley, CA

Ben Whipker
Rochester Institute of Technology
Rochester, NY

Steve Wilkinson
Juniper Networks
Sunnyvale, CA

Joseph Williams
EMX Industries, Inc.
Cleveland, OH

Brian Wright
Keysight Technologies
Santa Rosa, CA

Darien Yeang
Keysight Technologies
Santa Rosa, CA, Malaysia

Bill Yeap
KYZEN Sdn. Bhd.
Bayan Lepas, Penang, Malaysia

Aik Keong Yeoh
GOOGLE
New Taipei City, Taiwan

Bryan Young
Sensus
Morrisville, NC

Kevin Zhang
Cisco
SHENZHEN, China

Sunny Z Zhang
Juniper Networks
Shanghai, China

Alice Zilioli
SPEA SpA
Volpiano, Italy

Global Members

Amazon

Celestica, Inc.

Collins Aerospace

Creation Technologies Inc.

Henkel Electronic Materials LLC

HISCO, Inc.

IDENTCO

INVENTEC Performance Chemicals

ITW EAE

Juniper Networks

Keysight Technologies

KYZEN Corporation

L3HARRIS

Lenovo System Technology Company Limited, Shenzhen, PRC

MacDermid Alpha Electronics Solutions

Metallic Resources, Inc.

Micro Systems Technologies Management AG

NEO Technology Solutions

Nokia Bell Labs

Plexus Corp.

Samtec

Specialty Coating Systems, Inc.

VEXOS

ZESTRON Americas

Corporate Members

4Front Solutions
Palm Bay, FL

4Front Solutions
Erie, PA

5N Plus Micro Powders
Montreal, QC, Canada

A. I. Technology Inc.
Princeton Jct., NJ

AB Electronics Inc
Brookfield, CT

AbelConn, LLC
New Hope, MN

ACC Electronix, Inc.
Normal, IL

Accu-Automation Corporation
Waterloo, ON, Canada

Acculogic Inc.
Markham, ON, Canada

Accurate Technologies, Inc.
Novi, MI

ACDi
Frederick, MD

ACI Technologies, Inc.
Philadelphia, PA

ACL STATICIDE
Maple Grove, MN

Acuity Brands Lighting
Guadalupe, NL, Mexico

Adam Electronics
Madison Heights, MI

ADCO Circuits, Inc.
Rochester Hills, MI

Advance Circuit Technology, Inc.
Rochester, NY

Aegis Software
Horsham, PA

AGCO GRAIN & PROTEIN
St-Hubert, Canada

AGI Corporation
Huntsville, AL

AIM - Soldadura de Mexico S.A. de C.V.
Juarez, CH, Mexico

AIM Solder
Cranston, RI

Air Products and Chemicals, Inc.
Allentown, PA

Akrometrix LLC
Atlanta, GA

All Flex Flexible Circuits
Bloomington, MN

Allendale Electronics Ltd.
Lockeport, NS, Canada

Allfavor Technology
Schaumburg, IL

Alliance Rubber Company
Hot Springs, AR

Alltemated
Arlington Heights, IL

Altek Electronics, Inc.
Torrington, CT

Altron, Inc.
Anoka, MN

Altronic, LLC (A Member of the Hoerbiger Group)
Girard, OH

Amazon
Sunnyvale, CA

Amazon AWS
Sugar Land, TX

America II Electronics LLC
St. Petersburg, FL

American Hakko Products, Inc.
Valencia, CA

American Standard Circuits, Inc.
West Chicago, IL

American Technology Components Inc.
Elkhart, IN

Amitron Corporation
Elk Grove Village, IL

Amkor Technology, Inc.
Tempe, AZ

Amphenol Borisch Technologies
Grand Rapids, MI

Ampthink
Garland, TX

AMTI
Lynchburg, VA

Analog Technologies Corporation
Burnsville, MN

ANDA TECHNOLOGIES USA INC
Fremont, CA

Annapolis Micro Systems, Inc.
Annapolis, MD

APAG Elektronik
Windsor, ON, Canada

Apollo Seiko
Bridgman, MI

Apollos Industries
Orange, CA

Appareo
Fargo, ND

Applicad Inc.
Farmingdale, NJ

Applied Technical Services
Sammamish, WA

Aqueous Technologies
Corona, CA

Arc-Tronics, Inc.
Elk Grove Village, IL

Argo Transdata
Clinton, CT

ASC International
Medina, MN

Ascentec Engineering
Tualatin, OR

Ascentron, Inc
White City, OR

ASM Assembly Systems
Suwanee, GA

Astronautics Corporation of America
Milwaukee, WI

ASYS Group Americas Inc.
Suwanee, GA

Austin American Technology Corporation
Burnet, TX

Aven, Inc.
Ann Arbor, MI

AVID Associates Inc.
Flemington, NJ

Axiom Electronics LLC
Hillsboro, OR

BAE Systems
Austin, TX

Bare Board Group
Largo, FL

BBM, Inc.
McKinney, TX

Benchmark Electronics, MN Division
Winona, MN

Bently Nevada LLC
Minden, NV

BEST Inc.
Rolling Meadows, IL

Bestronics, Inc.
San Jose, CA

BGA Test & Technology
Bohemia, NY

Bittele Electronics Inc.
Markham, ON, Canada

Blackfox Training Institute
Longmont, CO

Bleam Group Limited
ShenZhen, China

BlueRing Stencils
Lumberton, NJ

BOFA Americas, Inc.
Staunton, IL

Brock Electronics Ltd.
Kanata, ON, Canada

BSE INC
Schaumburg, IL

BTU International
North Billerica, MA

BTW Inc.
Coon Rapids, MN

Burton Industries, Inc.
Hazelhurst, WI

CAMtek, Inc.
Bloomington, IL

Canon USA, Inc.
San Jose, CA

CareHawk Inc.
Kitchener, ON, Canada

Carlton Industries Corporation
Hamden, CT

CCL Design
Wheaton, IL

Celestica, Inc.
Toronto, ON, Canada

CEMSI
Weyers Cave, VA

CheckSum LLC
Arlington, WA

Circuit Check Inc.
Maple Grove, MN

Circuit Works Corporation
Waukegan, IL

CIRCUITS ASSEMBLY Magazine
Amesbury, MA

CMC Electronics Inc.
St. Laurent, QC, Canada

CO-AX Technology, Inc.
Solon, OH

Cobar Solder Products
Altoona, PA

Collins Aerospace
Rockford, IL

Colonial Electronic Manufacturers Inc.
Nashua, NH

Communications Security Establishment
Ottawa, ON, Canada

Computrol Meridian
Meridian, ID

Computrol, Inc.
Westminster, CO

Comtech PST
Melville, NY

Comtest Networks Inc.
Ottawa, , Canada

Comtree Inc.
Mississauga, ON, Canada

Condair Inc.
Sturtevant, WI

Conductive Containers
New Hope, MN

Conecsus LLC
Terrell, TX

Conecsus LLc Mexico
, Mexico

Contemporary Controls
Downers Grove, IL

ControlTek
Vancouver, WA

Corfin Industries LLC
Salem, NH

Cornet Technology
Springfield, VA

Count-On Tools, Inc.
Gainesville, GA

CPAC Systems AB
NA Molndal, Sweden

Creation Technologies Inc.
Markham, ON, Canada

Creative Electron, Inc.
San Marcos, CA

Crown Equipment Corporation
New Bremen, OH

Crystal Mark, Inc.
Glendale, CA

CTI Systems
Sanford, NC

CTrends
Foothill Ranch, CA

Cumberland Electronics
Harrisburg, PA

CyberOptics Corporation
Minneapolis, MN

Daktronics, Inc.
Brookings, SD

Datest Corporation
Fremont, CA

Datum Alloys
Endicott, NY

DCA Manufacturing Corporation
Cumberland, WI

DEKRA iST Reliability Services Inc.
Hsinchu City, Taiwan

DEN-ON INSTRUMENTS CO., LTD
Tokyo, Japan

DG Marketing Corporation
Austin, TX

Digitaltest, Inc.
Concord, CA

Dimation
Shakopee, MN

Dorigo Systems Ltd.
Burnaby, BC, Canada

Ducommun Incorporated
Tulsa, OK

Dynalab, Inc.
Reynoldsburg, OH

E.T.S. Group, Inc.
Lake Forest, CA

Eastek International Corporation
Lake Zurich, IL

ECD
Milwaukie, OR

EEI Manufacturing Services
Clearwater, FL

EI Microcircuits, Inc.
Mankato, MN

ELANTAS PDG, Inc.
St Louis, MO

Electrolab, Inc.
Boerne, TX

Electrolube
Benbrook, TX

Electronic Assembly Products
Dayton, OH

Electronic Coating Technologies
Brampton, ON, Canada

Electronic Interconnect
Elk Grove Village, IL

Electronic Systems, Inc.
Sioux Falls, SD

Electronica Test Laboratories
Sugar Land, TX

Ellsworth Adhesives
Germantown, WI

Eltek USA Inc.
Manchester, NH

Emerson Machine Automation Solutions
Charlottesville,

Engent, Inc.
Norcross, GA

EO Technics International, Inc
Gilbert, AZ

Epoxy Technology Inc.
Billerica, MA

EPTAC Corporation
Manchester, NH

Esdman Co., Ltd.
Bao An District, Shenzhen, China

ESSEMTEC USA
Glassboro, NJ

Europlacer Americas'
Tampa, FL

EV Group, Inc.
Tempe, AZ

Excel Electronics Inc
Elkhart, IN

Express Manufacturing Inc.
Santa Ana, CA

Extant Aerospace
Melbourne, FL

Facebook
Menlo Park, CA

Fancort Industries, Inc.
West Caldwell, NJ

FCT Assembly, Inc.
Greeley, CO

Finetech
Gilbert, AZ

FINN Test Electronics
Lake Zurich, IL

Firstronic LLC
Grand Rapids, MI

FKN Systek, Inc.
Millis, MA

Flex
Colonia La Mora, Zapopan,, JA, Mexico

Flexible Circuits, Inc.
Warrington, PA

FlexLink Systems, Inc.
Allentown, PA

Foresite, Inc.
Kokomo, IN

FreeWave Technologies
Boulder, CO

Fuji America Corporation
Vernon Hills, IL

Fujitsu Networks Comunications
Richardson, TX

Fusion EMS
Hillsboro, OR

Gables Engineering Inc
Coral Gables, FL

Garland Service Company
Garland, TX

Garmin AT, Inc.
Salem, OR

Garmin International
Olathe, KS

GEN3 Systems
Farnborough, Hampshire, UK

General Microcircuits Inc.
Mooresville, NC

General Monitors, Inc.
Lake Forest, CA

Geospace Technologies
Houston, TX

GHSP
Grand Haven, MI

Glenbrook Technologies Inc.
Randolph, NJ

Google
Mountain View, CA

GPD Global
Grand Junction, CO

Grass Valley, a Belden Brand
Montreal, QC, Canada

Great Lakes Engineering
Maple Grove, MN

GreenSoft Technology, Inc.
Pasadena, CA

Hangzhou H3C Tech. Co., Ltd.
Hangzhou, Zhejiang Province, China

Hanwha Techwin Automation Americas. Inc.
Cypress, CA

Harimatec Inc.
Duluth, GA

Harman de Mexico S de RL de CV
Queretaro, Queretaro, Mexico

Henkel Electronic Materials LLC
Irvine, CA

Henkel US Operations Corp.
Prescott, WI

Hentec Industries Inc.
Otis Orchards, WA

HEPCO, Inc.
Sunnyvale, CA

Hi-Tek Electronics
Salem, OR

HISCO, Inc.
Houston, TX

Honeywell FM&T
Kansas City, MO

Houstech, Inc.
Houston, TX

Hughes Circuits, Inc.
San Marcos, CA

HumiSeal Europe Ltd.
Winnersh, , UK

HZO
Burlington, NC

I Source Technical Services, Inc.
Lake Forest, CA

I. Technical Services, LLC
Alpharetta, GA

IBM Canada Ltée
Bromont, QC, Canada

iBtest Innovative Board Test
Tlaquepaque, Jalisco, Mexico

ICAPE-USA
Kokomo, IN

IDENTCO
Ingleside, IL

IKEUCHI USA, INC.
Cincinnati, OH

IMI, Inc.
Haverhill, MA

Indium Corporation
Utica, NY

INGUN USA, Inc.
Clover, SC

Innovative Circuits, Inc.
Alpharetta, GA

Inovar, Inc.
North Logan, UT

Inovaxe Corporation
Deerfield Beach, FL

InsulFab PCB Tooling
Spartanburg, SC

Integrated Technology Limited
Markham, ON, Canada

Intel Corporation
Hillsboro, OR

International Control Services, Inc.
Decatur, IL

INVENTEC Performance Chemicals
Vincennes (Paris), France

IPS Assembly Corporation
Livonia, MI

IPTE, LLC
Alpharetta, GA

Isola Group
Jefferson, OH

iST-Integrated Service Technology Inc.
Hsinchu, Taiwan

ITM Consulting
Springfield, TN

Itron, Inc.
Waseca, MN

ITW Contamination Control
Kennesaw, GA

ITW EAE
Hopkinton, MA

J.W. Speaker
Germantown, WI

Jabil Circuit, Inc.
St. Petersburg, FL

Jabil Circuit, Inc.
Auburn Hills, MI

JBC Tools USA Inc.
SAINT LOUIS, MO

Jendco Technologies
Fort Wayne, IN

JH Technologies
Fremont, CA

JJ Technologies
Wareham, MA

John Deere Electronic Solutions, Inc.
Fargo, ND

Johnson Controls
North York, ON, Canada

Johnson Controls
Milwaukee, WI

Juniper Networks
Sunnyvale, CA

K & F Electronics, Inc.
Fraser, MI

Kapsch TrafficCom
Mississauga, ON, Canada

Keysight Technologies
Georgetown, Penang, Malaysia

Keytronic
Oakdale, MN

KIC
San Diego, CA

Kimball Electronics Inc.
Jasper, IN

Kimco Distributing
Mentor, OH

Kinwong Electronic Co., Ltd
TLAJOMULCO DE ZUNIGA,JALISCO, Mexico

Koh Young Technology Inc.
Geumcheon-Gu, Seoul, , Republic of Korea

kolb CLEANING TECHNOLOGY GmbH
Willich, Germany

Kostal Ireland GMBH
Abbeyfeale, Co. Limerick, Ireland

Krayden, Inc.
Denver, CO

Krypton Solutions
Plano, TX

Kulicke & Soffa Industries
Fort Washington, PA

Kurtz Ersa, Inc.
Plymouth, WI

KYZEN Corporation
Nashville, TN

L-3 Harris
Camden, NJ

L3HARRIS
Melbourne, FL

Lab Pro Inc
Sunnyvale, CA

LeeMAH Electronics
Richardson, TX

Leidos
Columbia, MD

LEL Semi
Duncan, SC

Lenovo System Technology Company Limited, Shenzhen, PRC
Shenzhen City, China

Lenze
Uxbridge, MA

Lexicon Technologies Inc
Conyers, GA

Libra Industries, Inc.
Mentor, OH

Lockheed Martin
Oldsmar, FL

Lockheed Martin
Owego, NY

Logic PD, Inc.
Eden Prairie, MN

Logican Technologies
Edmonton, AB, Canada

LPKF Laser & Electronics
Tualatin, OR

M-Wave International, LLC
Glendale Heights, IL

MacDermid Alpha Electronics Solutions
Waterbury, CT

Mack Technologies Inc.
Melbourne, FL

MacroFab
Houston, TX

Magnalytix
Nashville, TN

MAGNEKON, SA DE CV
SAN NICOLAS DE LOS GARZA, NL, Mexico

Manncorp
Huntingdon Valley, PA

Maqim SA de CV
Tlajomulco de Zuñiga, JA, Mexico

Master Bond Inc.
Hackensack, NJ

Mat-tech
NL-5692 DM Son,, Netherlands

Matric LTD
Seneca, PA

MBDA (UK)
Bolton, , UK

MEC A/S
Ballerup, , Denmark

MELECS Electronics Queretaro
Querétaro, Querétaro, Mexico

Mellanox Technologies Ltd.
Yokneam, Israel

Mentor, a Siemens Business
Longmont, CO

Metallic Resources, Inc.
Twinsburg, OH

Metcal / OK International
Cypress, CA

MG Chemicals
Burlington, ON, Canada

Micro Systems Engineering, Inc.
Lake Oswego, OR

Micro Systems Technologies Management AG
Baar, Switzerland

MicroCare Corporation
New Britain, CT

Micron Corporation
Norwood, MA

Micron Technology, Inc.
Boise, ID

MicroScreen, LLC
South Bend, IN

Micross
Crewe, UK

Mid-America Taping & Reeling
Glendale Heights, IL

Mirac, LLC.
Lynchburg, OH

Miraco, Incorporated
Manchester, NH

Mirtec Corporation
Oxford, CT

MPI
Seymour, CT

MPL Inc.
Ithaca, NY

Mudisa Sa De CV
Tlajomulco de Zuniga, Jalisco, Mexico

Multicircuits Inc.
Oshkosh, WI

Murray Percival Company
Auburn Hills, MI

Mycronic, Inc
Rowley, MA

N.F. Smith & Associates, L.P.
Houston, TX

National Circuit Assembly
Garland, TX

National Instruments
Austin, TX

Naval Surface Warfare Center, Crane Division, (NSWC Crane)
Crane, IN

NEO Technology Solutions
Westborough, MA

Newtechnik Ind.Com.Prod.Eletr.ltda
Ribeirao Pires, , Brazil

NexGen Digital
Irvine, CA

Nihon Superior Company, Ltd.
Suita City, Osaka, , Japan

Nikon Metrology, Inc.
Brighton, MI

Nitto Kohki USA, Inc.
Roselle, IL

Nokia Bell Labs
Murray Hill, NJ

Norcott Technologies Ltd
Widnes, UK

Nordson ASYMTEK
Carlsbad, CA

Nordson DAGE
Aylesbury, Buckinghamshire,
Bucks, UK

Nordson EFD
East Providence, RI

Nordson SELECT
Liberty Lake, WA

Nordson Sonoscan
Santa Clara, CA

Northrop Grumman
Salt Lake City, UT

NPI Services, Inc.
Costa Mesa, CA

NPI Technologies, Inc.
Sugar Land, TX

nScrypt, Inc.
Orlando, FL

NTS-Baltimore
Hunt Valley, MD

Nu-Way Electronics, Inc.
Elk Grove Village, IL

Odyssey Electronics
Livonia, MI

OES, Inc.
London, ON, Canada

Omron Inspection Systems
Hoffman Estates, IL

Optimal Electronics Corporation
Austin, TX

OSDA Contract Services
Milford, CT

Out of the Box Manufacturing
Renton, WA

P. Kay Metal, Inc.
Los Angeles, CA

P4Q Electronics USA, Inc.
Albuquerque, NM

PA&LS, LLC
Trabuco Canyon, CA

PAC Global, Inc.
Dallas, TX

PAC Mexico
Guadalajara, JA, Mexico

PACE Worldwide
Vass, NC

PacTech USA Inc.
Santa Clara, CA

PacTech USA Packaging
Technologies Inc.
Santa Clara, CA

Palomar Technologies
Carlsbad, CA

PalPilot International Corporation
Englewood, CO

Panasonic
Rolling Meadows, IL 60008, IL

PARMI USA INC.
San Diego, CA

Parpro Technologies
Santa Ana, CA

Part Analytics
Brookfield, WI

PCB Connect Inc.
Sharon, MA

PCBA Supplies
Anna, TX

PDR Rework and Test Systems
Shingle Springs, CA

Peerless Instrument
East Farmingdale, NY

Pennatronics Corporation
California, PA

Pentagon EMS Corporation
Hillsboro, OR

Peters Research GmbH & Co. KG
Kempen, Germany

PFC Flexible Circuits
Mississiauga, ON, Canada

Photo Etch Technology, Inc.
Lowell, MA

Pillarhouse USA, Inc.
Elk Grove, IL

Pinnacle Technology Group
Ottawa Lake, MI

Pivot-DigitTron, Inc.
Shawnee, KS

Plexus Corp.
Neenah, WI

Polyonics
Westmoreland, NH

Powertrain Control Solutions
Ashland, VA

Practical Components
Los Alamitos, CA

Precision Technology, Inc.
Plano, TX

PRIDE Industries
Roseville, CA

Prime Technological Services, LLC
Suwanee, GA

Princeps Electronics Limited
Harlow, Essex, UK

Pro-Active Engineering, Inc.
Sun Prairie, WI

Process Sciences, Inc.
Leander, TX

Promex Industries, Inc.
Santa Clara, CA

Prototron Circuits
Redmond, WA

PVA
Cohoes, NY

QSC, LLC
Costa Mesa, CA

Qual-Pro Corporation
Gardena, CA

QUALITEK INTERNATIONAL, INC.
Addison, IL

Qualtech Technologies, Inc.
Willoughby, OH

Quik-Tool
Plainville, MA

Quiptech
Tlajomulco de Zuñiga, Jalisco,
Mexico

Raven Industries Inc.
Sioux Falls, SD

RBB Systems
wooster, OH

Rehm Thermal Systems LLC
Roswell, GA

Reliable Controls Corporation
Victoria, BC, Canada

Renishaw PLC
Chippenham, Wiltshire, UK

Repstronics, SA de CV
Zapopan, JA, Mexico

Retronix
Coatbridge, Lanarkshire, UK

RiverSide Electronics Ltd.
Lewiston, MN

Robert McKeown Company, Inc.
Branchburg, NJ

Robotas Technologies Ltd
Harrogate, UK

Rochester Institute of Technology
(RIT)
Rochester, NY

Rocktin Technology Canada
Richmond, BC, Canada

Rockwell Automation
Mayfield Heights, OH

Rockwell Automation
Mequon, WI

Rogers Electro-Matics
Syracuse, IN

Rolls-Royce Control Systems
Solihull, UK

Safari Circuits, Inc.
Otsego, MI

Saki America Inc.
Fremont, CA

Saline Lectronics, Inc.
Saline, MI

Samtec
New Albany, IN

Sanmina
Huntsville, AL

Saturn Electronics Corporation
Romulus, MI

SCHUNK Electronic Solutions
Morrisville, NC

SCHUNK Mexico
Querétaro, Mexico

Schweitzer Engineering Labs
Pullman, WA

Scienscope
Chino, CA

Scott Electrokrafts, Inc.
Andover, CT

Seagate Technology
Shakopee, MN

SEAKR Engineering, Inc.
Centennial, CO

Season Group
San Antonio, TX

SEC Co. Ltd
Suwon, South Korea, Republic of Korea

SEHO North America, Inc.
Erlanger, KY

Seica Inc.
Haverhill, MA

Seika Machinery, Inc.
Torrance, CA

SelecTech
Avon, MA

Semi-Kinetics
Lake Forest, CA

Senju Comtek Corporation
Santa Clara, CA

SHENMAO Technology, Inc.
San Jose, CA

Shenzhen Jufeng Solder Co., Ltd.
Longgang District, Shenzhen, China

SICK, Inc.
Minneapolis, MN

Sigmapoint Technologies Inc.
Cornwall, ON, Canada

Simplimatic Automation
Virginia, VA

SMART Microsystems
Elyria, OH

Smart Sonic
Cleveland, OH

Smart Splice, LLC
Surfside Beach, SC

SMarTsol Technologies
Zapopan, Jalsico, Mexico

SMT North America, Inc.
Richmond, VA

SMT Worldwide
Santa Catarina, NL, Mexico

SMTC
Melbourne, FL

SMTo Engineering
Tlaquepaque, JA, Mexico

SMTVYS LLC
El Paso, TX

SolarEdge Technologies
Herzeliya, Israel

Solder Indonesia, PT.
Cileungsi - Bogor, , Indonesia

SolderMask, Inc.
Huntington Beach, CA

SolderStar LLC
Clearwater, FL

Southwest Research Institute
San Antonio, TX

Sparton Onyx
Watertown, SD

SPEA America
Tyler, TX

SPEA SpA
Volpiano, , Italy

Specialty Coating Systems, Inc.
Indianapolis, IN

Spectra-Tech Manufacturing Inc
Batavia, OH

Spectrum AMT
Colorado Springs, CO

Speedprint Technology
Tampa, FL

SRC Tec
N Syracuse, NY

Stanley Healthcare
Lincoln, NE

STE-SEHO
Zapopan, Jalisco, Mexico

StenTech
GOLDEN, CO

STI Electronics, Inc.
Madison, AL

STIM Canada Inc.
Toronto, ON, Canada

Streamline Circuits LLC
Santa Clara, CA

Sunshine Global Circuits
Plano, TX

Super PCB
Plano, TX

Superior Flux & Manufacturing
Solon, OH

Surtek Industries Inc.
Surrey, BC, Canada

SÜSS MicroTec Inc.
Corona, CA

SVTronics, Inc.
Plano, TX

Synapse Electronique Inc.
Shawinigan, QC, Canada

Syncro Corp
Arab, AL

Sypris Electronics, LLC
Tampa, FL

Systems Innovation Engineering
Mullica Hill, NJ

TAGARNO USA
Greenwood, SC

Technica, USA
San Jose, CA

Technical Support Inc.
Omaha, NE

Technimark, Inc.
Cary, IL

Techtron Systems Inc.
Sohon, OH

Techvalley Co., Ltd.
Seaongnam-city, Republic of Korea

Tecnova Electronics Inc.
Waukegan, IL

Tek PAk, Inc.
BATAVIA, IL

Tektronix, Inc.
Beaverton, OR

Teligent EMS

Teradyne, Inc.
N. Reading, MA

Test Research, Inc.
Taipei, TA, Taiwan

Test Technology Associates
Carrollton,, TX

Texmac/Takaya, Inc.
McHenry, IL

The Jefferson Project
Orlando, FL

The Test Connection, Inc.
Hunt Valley, MD

Thermaltronics USA, Inc.
Great Neck, NY

Thread-Rite Screw Products
Chicago, IL

Tintronics
Huntsville, AL

TopLine
Milledgeville, GA

TouchPad Electronics LLC
Mukwonago, WI

Tracer Inc.
Golden, CO

Trans Tec America
Chandler, AZ

Transforming Technologies
Toledo, OH

Transition Automation, Inc.
, MA

Trenton Technology Inc.
Utica, NY

Trilogy Circuits, Inc.
Richardson, TX

Trylene, Inc.
Houston, TX

U-Bond Material Technology Co. Ltd.
Donguan City, Guangdong Province, China

UltraTape
WIlsonville, OR

Unison Industries
Jacksonville, FL

Universal Avionics
Tucson, AZ

Universal Instruments Corporation
Conklin, NY

V-TEK, Inc.
Mankato, MN

Valeo Detection Vision Systems
Co. Galway, Ireland

Valtronic Technologies (USA) Inc.
Solon, OH

Variosystems, Inc.
Southlake, TX

Venkel Ltd.
Austin, TX

Versa Electronics
Minneapolis, MN

VersaLogic Corporation
Tualatin, OR

VEXOS
Markham, ON, Canada

Virtual Industries Inc.
Colorado Springs, CO

Viscom
Zapopan, Jalisco, Mexico

Viscom Inc.
Duluth, GA

VisiConsult X-Ray Solutions
America Corp.
Atlanta, GA

Vision Engineering
New Milford, CT

VJ Electronix, Inc.
Chelmsford, MA

WAGO CORPORATION
Germantown, WI

Watchfire Signs
Danville, IL

Weller Tools
Lexington, SC

West-Tech Materials, Inc.
Costa Mesa, CA

WIN SOURCE ELECTRONICS
Hong Kong, China

WinTronics, Inc.
Sharon, PA

Yamaha
Kennesaw, GA

Yield Engineering Systems
Livermore, CA

Yxlon International
Hudson, OH

Zentech Manufacturing, Inc.
Baltimore, MD

ZESTRON Americas
Manassas, VA

Zollner Electronics Inc.
Milpitas, CA

ZTE Corporation
Shenzhen, , China

Zymet, Inc.
East Hanover, NJ

6600 City West Parkway, Suite 300
Eden Prairie, MN 55344 USA

Phone: +1-952-920-7682
Fax: +1-952-926-1819

E-Mail: smta@smta.org
Web site: www.smta.org